Master's Thesis

석사 학위논문

Magnetic Microrobot Locomotion in Vascular System Using A Combination of Time Delay Control and Terminal Sliding Mode Approach

Widya Aulia (위디야 아우리아)

Department of Robotics Engineering

DGIST

2014

Master's Thesis

석사 학위논문

Magnetic Microrobot Locomotion in Vascular System Using A Combination of Time Delay Control and Terminal Sliding Mode Approach

Widya Aulia (위디야 아우리아)

Department of Robotics Engineering

DGIST

2014

Magnetic Microrobot Locomotion in Vascular System Using A Combination of Time Delay Control and Terminal Sliding Mode Approach

Advisor: Professor Pyunghun Chang

Co-Advisor: Professor Bradley Nelson

by

Widya Aulia

Department of Robotics Engineering

DGIST

A thesis submitted to the faculty of DGIST in partial fulfillment of the requirements for the degree of Master of Science in the Department of Robotics Engineering. The study was conducted in accordance with Code of Research Ethics[1].

January 10th, 2014

Approved by

Professor Pyunghun Chang (Signature)

(Advisor)

Professor Bradley Nelson (Signature)

(Co-Advisor)

[1] Declaration of Ethical Conduct in Research: I, as a graduate student of DGIST, hereby declare that I have not committed any acts that may damage the credibility of my research. These include, but are not limited to: falsification, thesis written by someone else, and distortion of research findings or plagiarism. I affirm that my thesis contains honest conclusions based on my own careful research under the guidance of my thesis advisor.

Magnetic Microrobot Locomotion in Vascular System Using A Combination of Time Delay Control and Terminal Sliding Mode Approach

Widya Aulia

Accepted in partial fulfillment of the requirements for the degree of Master of Science.

December 10th, 2013

Head of Committee_____(Signature)

Prof. Pyunghun Chang

Committee Member_____(Signature)

Prof. Bradley Nelson

Committee Member_____(Signature)

Prof. Sangjun Moon

Degree

201223008

위디야 아우리아. Widya Aulia. Magnetic Microrobot Locomotion in Vascular System Using A Combination of Time Delay Control and Terminal Sliding Mode Approach. Department of Robotics Engineering. 2014. 51p. Advisors Prof. Chang, Pyunghun. Prof. Co-Advisors Nelson, Bradley.

Abstract

This thesis deals with designing a control law for trajectory tracking. The target is to move a microrobot in a blood vessel accurately. The microrobot is made of a ferromagnetic material and is propelled by a magnetic gradient coil.

The controller combines time delay control (TDC) and terminal sliding mode (TSM) control. TDC allows deriving a control law without prior knowledge of the plant. As the system is a nonlinear function which also includes uncertainties and unexpected disturbance, TDC gives a benefit of less effort needed compared to model-based controller. Meanwhile, TSM term adds accuracy which it compensates TDC estimation error and also adds robustness against parameter variation and disturbance. In addition, anti-windup scheme acts as a support by eliminating the accumulated error due to integral term by TDC and TSM. So, the proposed controller can avoid actuator saturation problem caused by windup phenomenon.

Simulations are conducted by copying a realistic situation. Accuracy and robustness evaluations are done in stages to see how each terms in a control law give an improvement and to see how an overall controller performs.

Keywords: Microrobot, trajectory tracking, time delay control, terminal sliding mode

CONTENT

LIST OF TABLES

LIST OF FIGURES

I. INTRODUCTION

1.1. BACKGROUND

Minimally invasive procedure, compared to traditional surgery, offers some benefits such as reduction of recovery time, medical complications, and infection risks.[1] Some notable inventions are da Vinci surgical robot and capsule endoscopy for gastrointestinal diagnosis. In recent years, there have been researches to further improve the procedure by reducing the size of the robot. A micro-scale robot is expected to allow the treatment to reach more remote locations which are inaccessible to existing tools. Although it is still in early concept, microrobots can be used for simple tasks such as drug delivery. This application has drawn the attention of many researchers.[2] A microrobot carrying drugs is controlled to precisely delivering drugs to target tissues or organs for treatment. Some critical needs for controlled drug delivery are cancer, AIDS, and brain disease treatment.

Drug delivery can be done by controlling the microrobot to get to the target through vascular system. Vascular system is arguably the most important application area for microrobot application as nearly every site of the body can be accessed by blood. However, a feedback control strategy for a device in the vascular system is quite challenging. Blood vessels' diameter are vary approximately from few μm in capillaries to 3cm in the aorta. There is also a nonnegligible blood flow whose variations in amplitude, waveform, and frequency from one blood vessel to another. Both add complexity in the conveyance of the device to the targeted area through a preassigned path.

The selected environment influences the design of the microrobot design, such as its size, shape, and material. The size can be made large enough to avoid Brownian Effect or small enough to be able to reach capillary. For shape choices, Arcese et.al [3] already made a research to figure out what shape is better for each vessel's region. In their work, the microrobot is made from ferromagnetic material and is propelled by a magnetic actuator. Magnetic systems is proven to be suitable for micromachine.[4] It can supply the magnetic field to the limited area by which the micromachine works wirelessly. Then, as blood vessels has a complex pathway, an untethered implementation is suitable to reduce the risks of tissue damages caused by the friction a tethered wire.[5]

Challenges also come from technology limitation. After the environment and the microrobot are determined, an actuator that can move the microrobot has to be available. Mathieu et al. proposed on using the magnetic gradient coils of an MRI.[6] They show that MRI can provide a necessary force to propel the microrobot. Since the application target is for medical purpose, a clinical MRI device provides some advantages. MRI devices are widely installed. It also provides imaging, human interface, real-time navigation system, and other functions for a complete system of propulsion method. However, due to an unpredictable natural environment, an unexpected disturbance may present; which if it is too big, the actuator may ended up cannot provide enough actuation to compensate it. Another challenge is the sensor measurement noise. The noise from sensor is usually in high frequency region. This could cause a chattering in the controller output which forces the actuator to reach saturation faster.

In order to overcome those challenges, a robust controller is required in order to ensure a smooth conveyance of the microrobot and to avoid collisions and/or friction to vessels walls. It has to be able to accurately and safely move the robot to the target location while maintaining its robustness against disturbances and noises. Some work has been done in this field.[7-10] However from the latest work of Arcese et.al[10], because the controller is a model-based, it is susceptible to modeling error.

The necessity of using a model-free controller leads us to using time delay control (TDC). TDC uses time delay estimation (TDE) which is able to estimate nonlinear function by assuming the change is not much in a sufficiently small time period.[11] This enables us to build a controller without fully knowledgeable of the system dynamics. Unfortunately, this advantage is limited by the practical implementation which can cause an estimation error. Therefore, terminal sliding mode (TSM) control is integrated to the controller. TSM is known for its robustness. It provides a fast error convergence which will improve the quality of the tracking.[12] This combination between TDC and TSM is first introduced by Maolin et al.[13] It is proven to be stable and robust against noise. As both TDC and TSM includes integral action, windup effect may occured. To avoid a saturation, anti-windup scheme will be integrated to the controller.

1.2. RELATED RESEARCH

Some researches have been done related to controlling a microrobot in blood vessels by using an MRI as an actuator. Tamaz et al. studies about the impact of a real-time MRI-based propulsion and tracking system constraints on the step response using a discrete PID controller.[7] A PID controller is selected for its simplicity while allowing easy identifications of the physiological and technological constraints. The simulation was done by taking accounts of MRI limitation while keeping the model simple. Some limitations included are the maximum magnetic gradient, overheating possibility, dead-time, and delay. They shows that the sampling period is important to determine an optimal navigation. Also, as the delay gets closer to the sampling frequency, the step response is becoming more deteriorated.

PID controller from Tamaz et al.[7] is further applied in an experiment.[14-17] In vivo automatic navigation of a ferromagnetic bead inside a carotid artery of a living swine proves that this controller is acceptable.[15] Here, a balloon catheter is used to stop the blood flow. In vitro experiment mimic in vivo behaviour is then conducted.[16] However when blood flow is added, the performance is deteriorated. The system is oscillating near the equilibrium point. It shows that the distance between two point, initial and target, needs to be made close to keep the bead not drifted to far away from the trajectory. However when two points are divided into some small segments, the ripple becomes bigger as it requires more localization and so more delay. Morever, due to the variation of physiological parameters, the writer indicates that the controller need to be retuned to keep it stable. Therefore, an algorithm to improve its robustness is needed.

Arcese et al. improves the control method by using backstepping method with high gain observer.[8] In their work, they pursue more complex plant modeling with a more relaxed MRI constraints. MRI constraints are further addressed in high level controller which is outside this thesis coverage. Backstepping controller guarantees the stability of the system while high gain observer provides velocity information required by the controller. This controller is proven to be stable but sensitive to small parameter error.

Arcese further improve the tracking quality and robustness by adding adaptive method and the use of MEMS force sensor.[9, 10] Adaptive controller and force sensor will calculate two most sensitive parameters, dielectric constant of blood and the magnetization of the microrobot respectively. In result, neither the stability of the closed-loop system nor the convergence of the observer are affected by parametric errors. Nevertheless,

the transient phase is critical since the actuator reaches saturation, estimated parameters are not updated, and the observers have not yet converged.

1.3. OBJECTIVE

The objective of this research is to develop a control scheme that can safely move the robot through blood vessels and accurately reach the target location despite uncertainties and disturbances from the environment. The controller must be robust against measurement noise. In addition, the control command must be kept inside the actuator limit.

1.4. SPECIFICATION

The specification of the overall system is as follows:

a. Plant
   - Structure: Sphere bead
   - Environment: Blood vessel
     - Inner diameter: 2 mm
     - Maximum blood-flow speed: 100mm/s

b. Actuator
   - Linear
   - Power: Magnetic field gradient
   - Maximum limit: ±70mT/mm

c. Sensor
   - Linear
   - Noise: ±0.1mm

d. Controller
   - Task:
     - Trajectory tracking
     - To avoid collision with vessel walls
   - Scheme: Time Delay Control and Terminal Sliding Mode

1.5. SCOPE

This research will focus on designing a control scheme for trajectory tracking of a microrobot. The only actuator constraint considered is its amplitude. The whole system, including the controller, the plant, the actuator, and the sensor, is modeled in Matlab. Simulation is conducted to confirm the stability and to test the performance of the controller.

1.6. OVERVIEW

This thesis has three chapters. Chapter 1 is an introduction for the research topic will be discussed. It covers the background of why this topic is chosen, followed by related researches, the research objective, the problem statement, the specification, and the research scope. Chapter 2 is an explanation of the method used to answer and to solve the problem. Advantages and drawbacks of the proposed method is also presented here. Then, it further explains the problem for the practical approach and available solutions. Chapter 3 includes simulations to prove the proposed method and discussions about the result.

II. METHOD

This thesis addresses and solves challenges step by step. The first challenge to be overcome is the difficulty of modeling an uncertain environment. Time delay control (TDC), with its estimation capability due to time delay estimation (TDE), allows the control law to be derived without knowing the plant model. The estimation accuracy is limited by the sampling rate from the microcontroller. This becomes the second challenge which will be compensated by integrating terminal sliding mode (TSM) to the controller. TSM is known for its robustness against disturbances. The third challenge is an actuator saturation. The maximum amplitude for the actuator is limited. There are some situations that may lead to saturation. One will be addressed here is a windup phenomenon. Since both TDC and TSM have integral function, both need an anti-windup to avoid this phenomenon. The fourth challenge is measurement noise.

2.1. TIME DELAY CONTROL (TDC)

TDC is chosen because it is a model-free controller. It doesn't require a prior knowledge of the plant equation as it intentionally uses previous information to estimate the current uncertainties. This estimation cancels the unknown dynamics and the unexpected disturbance with assumption that time-delay is sufficiently small.

The dynamic equation of a microrobot moving in a blood vessel is given by

$$m\ddot{p} = \overrightarrow{F_m} - \overrightarrow{F_d} - \overrightarrow{W_a} + d \qquad (2\text{-}1)$$

where m $\in \Re^n$ denotes the robot mass; $p \in \Re^n$ denotes robot's position which makes $\ddot{p} \in \Re^n$ the translational acceleration of the robot. $\overrightarrow{F_d} \in \Re^n$ represents the hydrodynamic drag force, $\overrightarrow{W_a} \in \Re^n$ is the apparent weight that includes the robot's weight and buoyancy force, $\overrightarrow{F_m} \in \Re^n$ stands for the magnetic force, and $d \in \Re^n$ is disturbance.

The magnetic force will be generated by using a field gradient by following an equation

$$\overrightarrow{F_m} = V_m(\vec{M}.\nabla)\vec{B} \tag{2-2}$$

where V_m is the robot's total volume, $\vec{M}$ is the magnetization of the robot, and $\vec{B}$ is the external magnetic field. By substituting $\overrightarrow{F_m}$ in (2-1) with (2-2), we have

$$m\ddot{p} = (\vec{M}.\nabla)\vec{B} - \overrightarrow{F_d} - \overrightarrow{W_a} + d \tag{2-3}$$

Let the input command $u = \nabla\vec{B}$ and rearrange (2-3):

$$u = {V_m}^{-1}\vec{M}^{-1}m\ddot{p} + {V_m}^{-1}\vec{M}^{-1}(\overrightarrow{F_d} + \overrightarrow{W_a} - d) \tag{2-4}$$

$$u = G\ddot{p} + G(\overrightarrow{F_d} + \overrightarrow{W_a} - d) \tag{2-5}$$

where

$$G = {V_m}^{-1}\vec{M}^{-1} \tag{2-6}$$

Introducing a constant diagonal matrix, $\bar{G}$, which represents the known part of G, one can obtain another expression of (2-5) as follows:

$$u = \bar{G}\ddot{p} + H \tag{2-7}$$

where H denotes the total sum of nonlinear dynamics of the robot and is described by:

$$H = G(\overrightarrow{F_d} + \overrightarrow{W_a} - d) + (G - \bar{G})\ddot{p} \tag{2-8}$$

The control objective is to find a input command u such that the tracking error, $e = p_d - p$, satisfies the following error dynamic:

$$\ddot{e} + K_d\dot{e} + K_p e = 0 \tag{2-9}$$

where $e = p_d - p$ denotes the position error vector with p_d denoting the desired position, $K_d \in \Re^n$ the derivative gain matrix, and $K_p \in \Re^n$ the proportional gain matrix. K_d and K_p are usually set to be positive, definite diagonal matrices.

Let $\widehat{H}$ as the estimation of term H which makes (2-7) becomes

$$u = \bar{G}\ddot{p}^* + \hat{H} \tag{2-10}$$

$$\ddot{p}^* = \ddot{p}_d + K_d\dot{e} + K_p e \tag{2-11}$$

Basically, the control in (2-10) attempts to cancel H in (2-7) by $\hat{H}$ and inject a desired dynamics in (2-11).

Assuming H is continuous or piecewise continuous and there is a sufficiently small sampling time, $\hat{H}$ can be estimated by using TDE as

$$H \cong H_{t-L} \triangleq \hat{H} \tag{2-12}$$

where subscript t-L denotes time-delayed value and L is the estimation time delay, usually equals to the sampling time. (2-12) is the essential idea of the TDC. TDE can be derived from (2-10) as follows

$$H_{t-L} = u_{t-L} - \bar{G}\ddot{p}_{t-L} \tag{2-13}$$

$$u = \bar{G}\ddot{p}^* - \bar{G}\ddot{p}_{t-L} + u_{t-L} \tag{2-14}$$

Then, injecting the desired dynamic into (2-14), the TDC law is obtained as follows:

$$u = \bar{G}\left(\ddot{p}_d + K_d\dot{e} + K_p e\right) - \bar{G}\ddot{p}_{t-L} + u_{t-L} \tag{2-15}$$

L should be small enough for TDC to meet the desired error dynamics of (2-9). However, the smallest achievable value of the sampling period depends on practical digital implementation. This constraint causes time delay estimation error. The following relationship is derived from substituting (2-12) into (2-10) and considering (2-7):

$$H - \hat{H} = H - H_{t-L} = \bar{G}(\ddot{p}^* - \ddot{p}) \tag{2-16}$$

The LHS of (2-16) denotes the estimation error. Let ε denotes the TDE error as follows:

$$\varepsilon \triangleq \bar{G}^{-1}(H - H_{t-L}) = \ddot{p}^* - \ddot{p} \tag{2-17}$$

Substituting (2-11) into (2-17), the closed-loop error dynamics of TDC becomes:

$$\varepsilon = \ddot{e} + K_d\dot{e} + K_p e \tag{2-18}$$

(2-18) shows the consequence of the TDE error, ε, on the desired error dynamics. ε causes the resulting dynamics to deviate from the desired error dynamics. Therefore, an additional term is required to compensate this error.

2.2. TERMINAL SLIDING MODE

Sliding mode control (SMC) system have been studied extensively and used in many applications due to their robustness and simplicity. The sliding mode is obtained by driving and then constraining the system states to lie within a neighborhood of the switching manifold. The dynamic behavior of the system can be determine by selecting a certain switching manifolds. When in the sliding, the closed-loop response becomes totally insensitive to both internal parameter uncertainties and external disturbances. In conventional SMC, the convergence of the system states to the equilibrium point is usually asymptoptical and not in finite time. Terminal sliding mode (TSM) controller is developed to address this problem.[12, 18, 19] This controller is particularly useful for high precision control as it speeds up the rate of convergence near an equilibrium point.

Similar to SMC, TSM also suffers chattering due to discontinuous control law. Yu et al. proposed a continuous finite-time control.[19] In his paper, the finite time convergence property of TSM is applied in both the reaching phase and the sliding phase of the sliding mode control system. As a result, the closed-loop system is globally finite-time stable and the trajectory-tracking objective is achieved in finite time.

For those advantages, the TSM is added to previous TDC control law (2-15). It is expected that TSM can compensate the estimation error by TDC. Below, the integration of TSM term into TDC will be derived which begun with choosing the sliding manifold. Following the work of Maolin et al.[20], the integral of the TDC desired dynamics is selected as follows

$$x(t) = \int \left(\ddot{e} + K_D \dot{e} + K_p e\right) dt = 0 \tag{2-19}$$

$$x(t) = \dot{e} + K_D e + K_p \int e \, dt = 0 \tag{2-20}$$

where $e = p_d - p$ and $x(t)$ is the TSM sliding manifold.

Then taking into account a quadratic Lyapunov condition

$$V(s) = \frac{1}{2}x^2 > 0 \tag{2-21}$$

With x defined in (2-20), a nonlinear feedback control law u is determined with the constant $\varepsilon > 0$ in such a way that the time derivative $\dot{V}$ of the Lyapunov function becomes negative definite according to the condition

$$\dot{V}(s) = \frac{1}{2}\frac{d}{dt}x^2 = x\dot{x} \leq -\beta|x| \tag{2-22}$$

This condition guarantees asymptotically stable convergence towards the sliding surface x=0 with a minimum convergence rate β.

$$x\dot{x} = x\left(\ddot{e} + K_D\dot{e} + K_p e\right) \tag{2-23}$$

$$x\dot{x} = x\left(\ddot{p}_d - \ddot{p} + K_D\dot{e} + K_p e\right) \tag{2-24}$$

$$x\dot{x} = x\left(\ddot{p}_d - (\bar{G}^{-1}(u - \mathrm{u_{t-L}}) + \ddot{p}_{t-L}) + K_D\dot{e} + K_p e\right) \tag{2-25}$$

A TSM control can be designed as

$$u = u_{t-L} + \bar{G}\left(\ddot{p}_d - \ddot{p}_{t-L} + K_D\dot{e} + K_p e + K_{tsm}|x|^{\gamma} sign(x)\right) \tag{2-26}$$

where $K_{tsm} > 0$ and $0 < \gamma < 1$.

To see whether the control law can force the state to reach the manifold, control u in (2-25) is replaced with (2-26) yields

$$x\dot{x} = x\left(K_{tsm}|x|^{\gamma} sign(x)\right) = -K_{tsm}|x|^{\gamma+1} \leq -\beta|x| \tag{2-27}$$

Thus, the trajectory reaches the manifold x=0 in finite time and, once in the manifold, it cannot leave it.

To reduce chattering, a saturation function is used instead of the signum function:

$$u = u_{t-L} + \bar{G}\left(\ddot{p}_d - \ddot{p}_{t-L} + K_D\dot{e} + K_p e + K_{tsm}|x|^{\gamma} sat_{\phi}(\lambda x)\right) \tag{2-28}$$

with $sat_{\phi}(\lambda x) = \begin{cases} 1, & |x| \geq \phi \\ \lambda x, & -\phi < x < \phi \end{cases}$

where ϕ is the saturation limit and λ is the saturation width.

The error dynamic is derived by substiting (2-7) and (2-13) into the control law (2-28) as follow:

$$\bar{G}\ddot{p} + H = \bar{G}\ddot{p}_{t-L} + H_{t-L} + \bar{G}\left(\ddot{p}_d - \ddot{p}_{t-L} + K_D\dot{e} + K_p e + K_{tsm}|x|^{\gamma} sat_{\phi}(\lambda x)\right) \quad (2\text{-}29)$$

$$H - H_{t-L} = \bar{G}\left(\ddot{e} + K_D\dot{e} + K_p e + K_{tsm}|x|^{\gamma} sat_{\phi}(\lambda x)\right) \quad (2\text{-}30)$$

$$\ddot{e} + K_D\dot{e} + K_p e = \bar{G}^{-1}(H - H_{t-L}) - K_{tsm}|x|^{\gamma} sat_{\phi}(\lambda x) \quad (2\text{-}31)$$

$$\ddot{e} + K_D\dot{e} + K_p e = \varepsilon - K_{tsm}|x|^{\gamma} sat_{\phi}(\lambda x) \quad (2\text{-}32)$$

where ε is error dynamic of TDC.

2.3. ANTI-WINDUP SCHEME

The proposed controller combines TDC and TSM. When this controller is applied to the system with a saturation limit, windup phenomenon is observed, causing excessive overshoot and instability. Windup phenomenon is caused by error accumulation due to integral action. The proposed controller have two integral terms. One comes from time delay estimation of TDC. The other is from TSM. Therefore, two anti-windup scheme is needed.

Chang et al.[21] have researched on the design of an anti-windup scheme for TDC as shown in Fig.2-1. A saturation function is added to the controller. The idea is to limit the input to the actuator so it may stay within the actuator limit. In the meantime, the time-delayed value of the limited u is used to produce u, thereby error accumulation can be prevented.

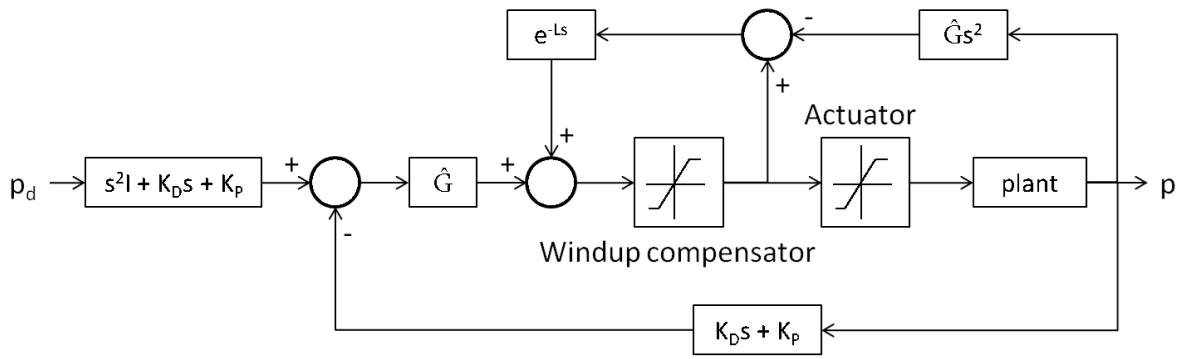

Figure 2-1. *Anti-windup scheme of TDC.*

Second anti windup is for integration in TSM. The method used is a tracking anti-windup, which is the classical method to prevent integral windup.[22] It is commonly described as shown in Fig.2-2. Once the controller output exceeds the saturation limit, the difference of saturated output and unsaturated output is fed back through a gain to reduce the amount of error input going into integrator in TSM.

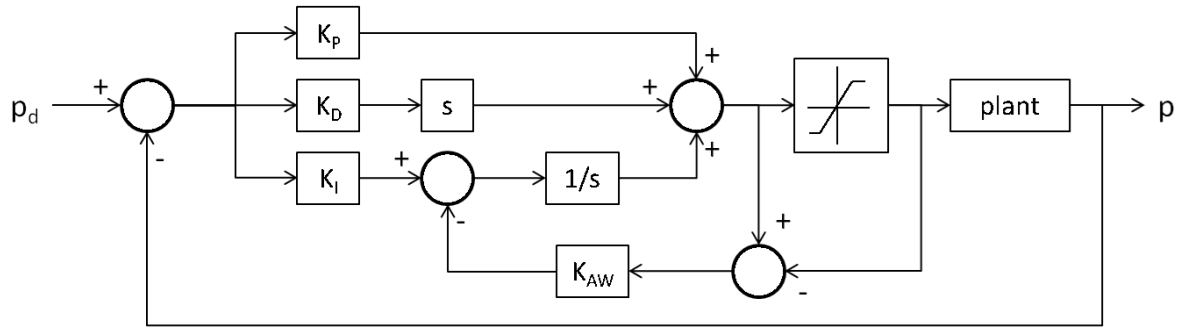

Figure 2-2. *Standard structure of a tracking anti-windup PID controller.*

After anti-windup scheme is added to the proposed controller, the final proposed control law becomes as follows:

$$u = u^*_{t-L} + \bar{G}\left(\ddot{p}_d - \ddot{p}_{t-L} + K_d\dot{e} + K_p e + K_{tsm}|x'|^\gamma sat_1(\lambda x')\right) \qquad (2\text{-}29)$$

with

$$x' = \dot{e} + K_d e + K_p \int \left(e + K_{aw}(u^* - u)\right) \tag{2-30}$$

and

$$u^* = sat_{|umax|}(u) \tag{2-31}$$

where u is the unsaturated input, u^* is the saturated input, x' is the modified sliding manifold, and *umax* is the saturation limit for the controller command. (2-29) can also be described as shown in Fig.2-3.

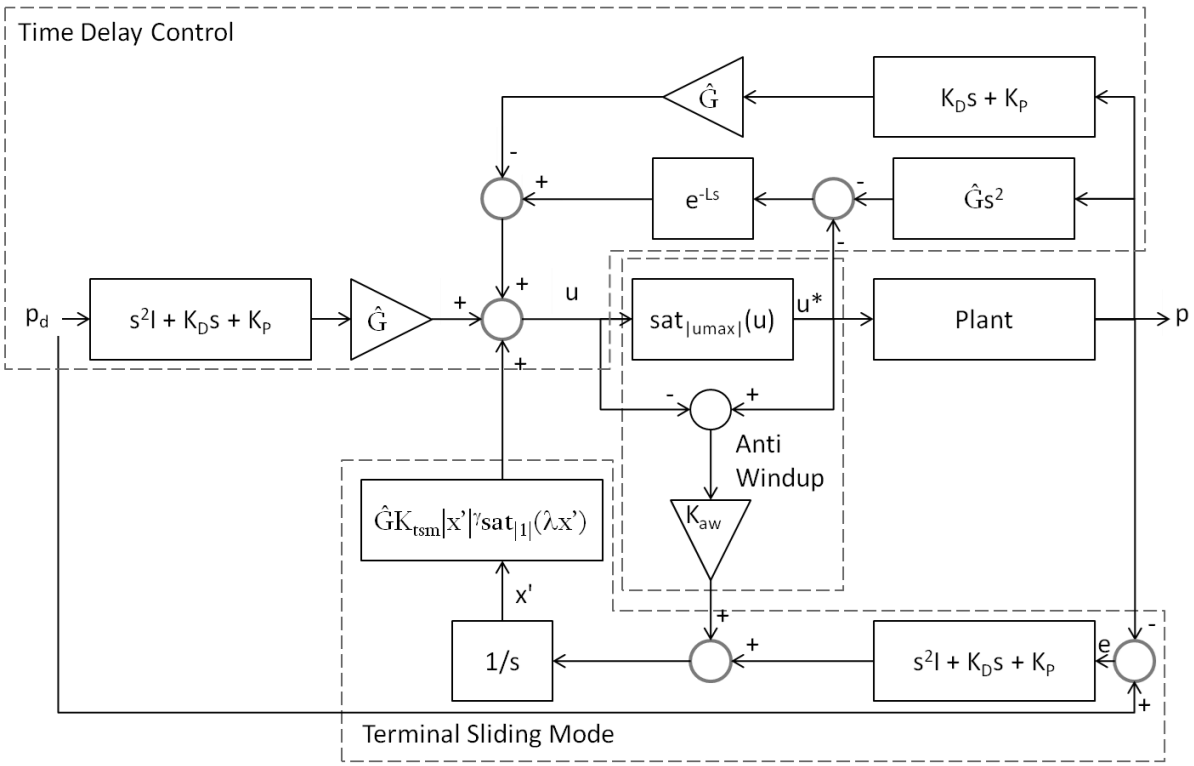

Figure 2-3. *A block diagram to represent the control law. There are three main blocks which are divided by dash lines (- -): Time delay control (TDC), terminal sliding mode control (TSM), and anti-windup scheme block. TDC works to eliminate all nonlinearities in the subsystem. It estimates the current unknown value by utilizing the previous information. TSM controller works to reduce the TDC estimation error and to force the position error, e, to converge in finite time. Anti-windup scheme is added to keep the control output, u, in the limit of the actuator. K_d and K_p value determine the error convergence rate. G, K_{tsm}, γ, and λ value are also user-defined which are needed to be tuned to get the best controller performance. K_{aw} is the last value to get tuned to optimize the anti-windup scheme.*

2.4. PRACTICAL APPROACH

2.4.1. FEEDBACK SIGNAL

The final proposed control law requires the knowledge of the robot's velocity and acceleration in addition of its position. In practice, the velocity and acceleration signals can be calculated by numerical differentiation as

$$\dot{p} = \frac{p - p_{t-L}}{L} \tag{2-32}$$

and

$$\ddot{p} = \frac{p - 2p_{t-L} + p_{t-2L}}{L^2} \tag{2-33}$$

where p, $\dot{p}$, and $\ddot{p}$ stands for position, velocity and acceleration respectively. L is the time delay.

2.4.2. CONTROLLER GAIN SELECTION

The proposed controller has five gains (K_d, K_p, $\bar{G}$, K_{tsm}, γ, and K_{aw}). This helps simplify the design procedure, which is briefly introduced as follows:

1. Determine the target sliding manifold by selecting K_d and K_P values.
2. Select a sampling time L with consideration of the controller hardware. Choose the nominal value as small as possible because it is related to the TDE error.
3. Set other gain (K_{tsm}, γ, and K_{aw}) to zero. Then tune $\bar{G}$ from small positive value and gradually increase it while checking the control performance by trial and error.
4. Set the width of the saturation function in TSM term, λ. Big value causes a fast convergence rate but weak against chattering.
5. K_{tsm} and γ should be tuned further to achieve the optimal performance.
6. Tune K_{aw} by observing the actuation performance. If no saturation happens, this compensation gain is redundant. However, if there is a saturation, gradually increasing it until the best performance is obtained.

2.4.3. MEASUREMENT NOISE

In practical applications, the feedback signal is always contaminated by noise. The noise effect can be amplified by derivative action. As the system is second order and so TDE requires twice numerical differentiation in order obtaining velocity and acceleration information. This makes the proposed controller is prone to noise.

In the literature related to TDE, there are three remedies for such problem. The first remedy is by adding an observer to reconstruct unmeasured states.[23, 24] However it adds complexity as it brings additional parameters to tune the performance. The second remedy is by using a low pass filter.[25] Third is by using a smaller value of TDC gains, $\bar{G}$.[26] This remedy has the same effect as using a first order digital LPF for the input command, which means that the third remedy has the same effect as the first remedy. This can be clarified by rewriting the proposed controller law as

$$\mathrm{u} = \bar{G}v - \bar{G}\ddot{p}_{t-L} + \mathrm{u}_{\mathrm{t-L}} \tag{2-34}$$

$$v = \ddot{p}_d + K_d\dot{e} + K_p e + K_{tsm}|x|^{\gamma} sat(\lambda x) \tag{2-35}$$

If a digital LPF with a cutoff frequency τ is added to the controller, the control law is modified as follows:

$$u^f = \frac{\tau}{1+\tau}u + \frac{1}{1+\tau}u^f{}_{t-L} \tag{2-36}$$

where u denothes the input to the filter and u^f the output from the filter. Substituting (2-34) into (2-36), the following filtered control law is obtained:

$$u^f = u^f{}_{t-L} + \frac{\tau}{1+\tau}\bar{G}(v - \ddot{p}_{t-L}) \tag{2-37}$$

Comparison of (2-29) and (2-37) shows that lowering controller gain value has the same effect with LPF.

2.5. ADVANTAGES AND DRAWBACKS

The proposed controller is robust against parameter variations and disturbances The proposed controller assures fast convergence due to the TSM and provides model-free control due to the TDE. Nevertheless, it doesn't free from drawbacks. This controller is sensitive to noise in feedback signal due to the use of numerical differentiation. Both advantages and drawbacks will be studied in the simulation in Chapter 3.

III. RESULTS

Simulations are performed to evaluate the controller proposed in terms of its capability to deal with uncertainties, scaling issue, and noise. It will be done in Matlab R2012A.

There are two trajectories used in the simulation. One is where the microrobot is controlled to move in one-dimension. Here, three simulations are conduction. First simulation is done to show the accuracy and the robustness of the proposed controller. Second simulation is done with a consideration of the actuator limitation. Here will be shown how anti-windup scheme integration to the controller can help to reduce the windup effect due to double integration of TDC and TSM. Last simulation is about the performance against noise in position measurement.The other trajectory is where the mirorobot is moving on a plane.

3.1. SIMULATION SETUP

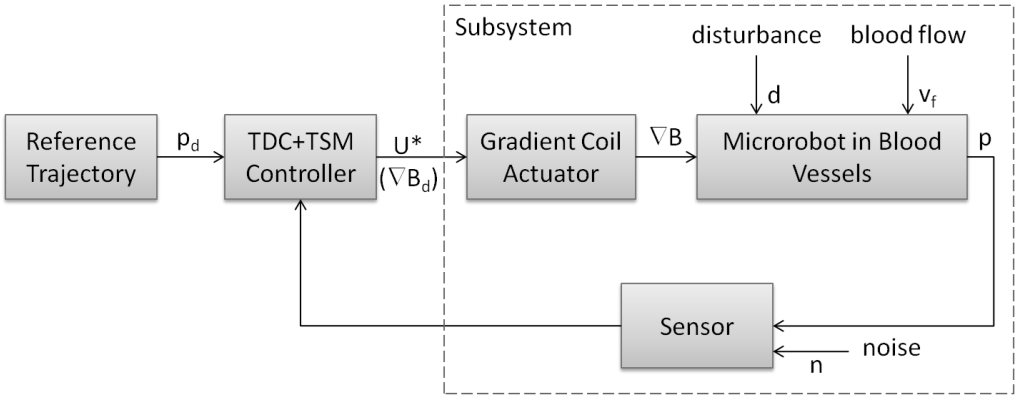

Figure 3-1. *A block diagram of a simplified model for overall system. The system is a trajectory tracking control system of a microrobot moving in a blood vessel.. It is divided into software (controller) and hardware. All physical models are collected into a subsystem. This subsystem includes the model of the magnetic coil actuator, the microrobot, the blood vessel environment, and the sensor. It also considers the blood flow. The purpose of this system is to make the microrobot follows the reference trajectory which is set by the user. By having a feedback from the microrobot actual position, p, the controller will calculate how much gradient magnetic field required (∇B_d) to move the microrobot to the desired position, p_d. The calculated value becomes the input command, u*, to the actuator.*

Fig.3-1 gives the simplified model of the system. It takes the form of a feedback system with the microrobot current position closing the loop. The overall system is divided into two big parts, software and physical environment. The software includes a controller and a trajectory generator while the physical environment consists of a magnetic coil actuator, a microrobot, and a blood vessel environment. The controller generates a command value by calculating the difference between the microrobot current position and the desired position. The actuator will take the command from the controller to generate the required magnetic field gradient and apply it to the microrobot.

3.1.1. PLANT MODELING

The plant of the system is a microrobot moving in a blood vessel moving along a determined trajectory. It takes a shape of a sphere bead. Sphere shape is chosen because this design is the best fitted to navigate in macrovasculature where the drag is important.[3]

Since the diameter of blood vessels is vary, these simulations will focus only for artery and arterioles. Inner diameter of the blood vessels is assumed to be 2mm and the microrobot will be placed in the middle of cross sectional area. It is expected for the microrobot not to deviate far from the center. Fluid flow is considered and will be modeled as a sine wave.

It is assumed the fluid is Newtonian incompressible and there is no turbulence. Another assumption is the microrobot doesn't change its orientation, also the size of it is large enough to neglect the effect the Brownian effects.

The translational motion of the robot moving in a fluid is as follows:

$$m\ddot{p} = \overrightarrow{F_m} - \overrightarrow{F_d} - \overrightarrow{W_a} + d \tag{3-1}$$

where m is the robot mass and p is its position which makes $\ddot{p}$ is the translational acceleration of the robot. $\overrightarrow{F_d}$ represents the hydrodynamic drag force, $\overrightarrow{W_a}$ is the apparent weight, $\overrightarrow{F_m}$ stands for the magnetic force, and d is the disturbance force. These forces, besides the disturbance, affect the microrobot motion as shown in Fig.2-2. Drag force is the resistance comes from the liquid caused by both the robot motion and also the fluid flow itself. Apparent weight is the combination of the robot's weight and the buoyancy force. Magnetic force is produced

by magnetic gradient which is generated by a gradient coil. It propels the microrobot to a target location. Magnetic force must be stronger than apparent weight combined with drag force of the blood flow on the microrobot for motion to take place and to allow control in displacement.

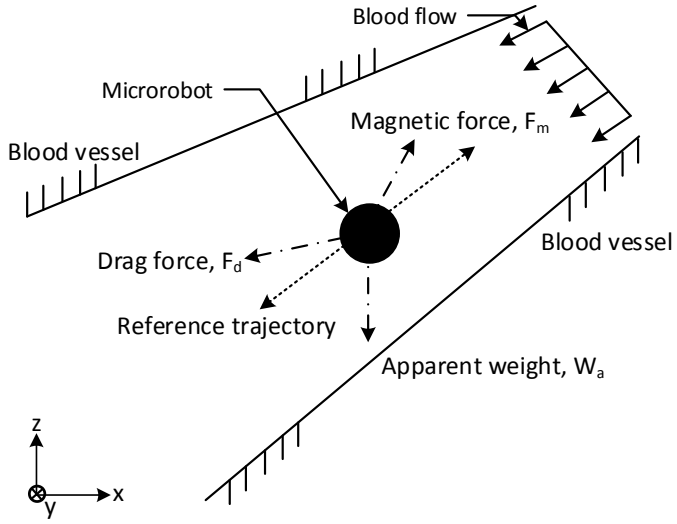

Figure 3-2. *Free body diagram for a microrobot moving in a blood vessel. The microrobot is expected to move back and forth following the reference trajectory which is represented by dash line (- -). The force acting on the microrobot is a summation of three forces generated from magnetic force (F_m), apparent weight (W_a), and drag force (F_d). Magnetic force is resulted by applying magnetic field gradient provided by a coil actuator to the microrobot. Drag force is caused by the motion of the microrobot. Apparent weight includes the microrobot weight and buoyancy force. Dash dot lines (-.-) represent forces acting on the microrobot. The figure is described on xz-plane with y-axis enters the paper.*

A. Magnetic Force

The magnetic force is a function of magnetic field gradient by following an equation

$$\overrightarrow{F_m} = \mu_0 V_m (\vec{M}.\nabla)\vec{B} \tag{3-2}$$

where $\overrightarrow{F_m}$ stands for magnetic force, μ_0 is permeability of free space ($4\pi\times10^{-7}$ H·m^{-1}), V_m is microrobot's volume, $\vec{M}$ is magnetization, and $\nabla\vec{B}$ is magnetic field gradient.

B. Drag Force

The hydrodynamic drag force for spherical bead is expressed as

$$\overrightarrow{F_d} = \frac{1}{2}\rho_f\left(v - v_f\right)^2 A C_d \frac{\overrightarrow{v-v_f}}{\|v-v_f\|} \tag{3-3}$$

where $\overrightarrow{F_d}$ stands for drag force, ρ_f is blood density, v is microrobot velocity, v_f is blood flow velocity, A is cross sectional area of the microrobot, and C_d is drag coefficient. This drag coefficient is a function of Reynold number, Re, and is given by [27]

$$C_d = \frac{24}{Re} + \frac{6}{1+\sqrt{Re}} + 0.4 \tag{3-4}$$

with Reynold number is as follows

$$Re = \frac{2\rho_f\|v-v_f\|r}{\eta} \tag{3-5}$$

where Re is Reynold number, r is radius of the microrobot, and η is blood viscosity.

C. Apparent Weight

As mentioned before, apparent weight is a net value of robot's weight and buoyancy force. It is expressed by

$$\overrightarrow{W_a} = V_m\left(\rho_r - \rho_f\right)\vec{g} \tag{3-6}$$

where $\overrightarrow{W_a}$ stands for apparent weight, V_m is for microrobot's volume, ρ_r is robot density, ρ_f is blood density, and $\vec{g}$ is gravitational acceleration.

3.1.2. ACTUATOR AND POSITION SENSOR MODELING

For simplicity, the actuator and the position sensor is assumed to be linear. Sensor in the simulation measures the position of the microrobot. The velocity and the acceleration value is obtained by using a numerical differentation.

3.1.3. TRAJECTORY

To keep the trajectory including its derivative, velocity, and its second derivative, acceleration, smooth, in this simulation, a quintic polynomial is used, namely

$$p(t) = a_0 + a_1 t + a_2 t^2 + a_3 t^3 + a_4 t^4 + a_5 t^5 \quad (3\text{-}6)$$

where solutions for six unknown constants, a_n, are given as

$$a_0 = p_0 \quad (3\text{-}7)$$

$$a_1 = \dot{p_0} \quad (3\text{-}8)$$

$$a_2 = \frac{\ddot{p_0}}{2} \quad (3\text{-}9)$$

$$a_3 = \frac{20p_f - 20p_0 - (8\dot{p_f} + 12\dot{p_0})t_f - (3\ddot{p_0} - \ddot{p_f})t_f{}^2}{2t_f{}^3} \quad (3\text{-}10)$$

$$a_4 = \frac{30p_f - 30p_0 + (14\dot{p_f} + 16\dot{p_0})t_f + (3\ddot{p_0} - 2\ddot{p_f})t_f{}^2}{2t_f{}^4} \quad (3\text{-}11)$$

$$a_5 = \frac{12p_f - 12p_0 - (6\dot{p_f} + 6\dot{p_0})t_f - (\ddot{p_0} - \ddot{p_f})t_f{}^2}{2t_f{}^5} \quad (3\text{-}12)$$

3.1.4. SIMULATION PARAMETER

A. Trajectory

The one-dimension simulation will cover the z-axis as it involves more terms compared to x-axis or y-axis; z-axis includes the weight of the robot and the buoyancy force. It will be done in 5 seconds. To see the performance in different conditions, this 5 seconds is divided into three parts. In the first 1.5 seconds, the microrobot will go to upper direction against the blood flow from the initial position to 10mm higher than the initial position. The next 2 seconds, it will be kept still on one position. Then in the last 1.5 seconds, it will go down to the initial position along with the blood flow.

This trajectory is shown in Fig.3-3. It is defined in high order polynomial as follows

$$p(t) = \begin{cases} 0.029t^3 - 0.029t^4 + 0.0079t^5 & 0 \le t \le 1.5 \\ 0.01 & 1.5 \le t \le 3.5 \\ -0.029t^3 + 0.029t^4 - 0.0079t^5 & 3.5 \le t \le 5 \end{cases} \quad (3\text{-}13)$$

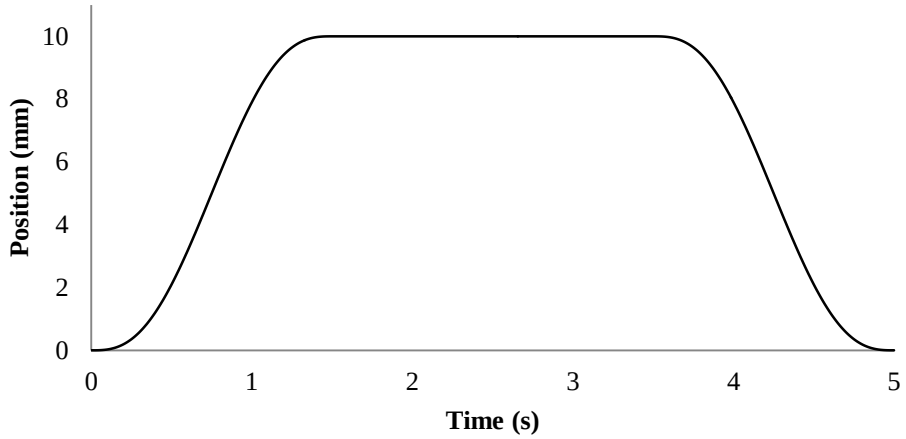

Figure 3-3. *Desired trajectory for Z-axis.*

For two-dimension simulation, the first section of trajectory equation will be reused and be applied for both x- and z-axises. It makes the microrobot moving 45^o to position (10,10)mm in 1.5 seconds

B. Plant Parameter Value

This simulation takes some values from previous research by Arcese et al.[8] The robot is made of ferromagnetic material with radius 300μm. This size is assumed to be big enough to avoid Brownian effect.

For the actuator limit, the required value and the available gradient coil are considered. The magnetic force need to be able to compensate the weight of the robot and also the drag force, especially when the robot moves against the flow. The minimum field gradient to move the bead against the flow when it is in the highest peak is:

$$F_{m_{min}} = |W_a + F_d| = (7.69 + 6.32) \times 10^{-6} = 14 \times 10^{-6} N \quad (3\text{-}14)$$

$$\nabla B_{min} = \frac{F_{m_{min}}}{(M \times V)} = 0.0635\ T/m \quad (3\text{-}15)$$

From the work by Mathieu et al.[6], Magnetic Resonance Imaging (MRI) systems are being considered as they provide the required magnetic fields and controls. Their imaging capabilities could also be used to track the displacements of the robots, providing position feedback informations. These days, MRI

can provide up to 80mT/m.[28] However, pushing the actuator to the limit can cause damage to it. Therefore, in this simulation, the actuator limit is set more constrained; that is 70mT/m. This is also in the purpose of showing the effectiveness of the anti-windup scheme and also to show that the proposed controller doesn't demand more than necessary.

C. Desired Dynamics

The desired dynamics of the controller is made critically damped. A critically damped response has a fastest response to reach a zero steady state error since it doesn't have an overshoot and an oscillations. The system is expected not to have an overshoot as it may cause a big error. Due to the small size of the blood vessels, a big error may cause damage to the wall. Therefore, Kd = 20 and Kp = 100 is chosen to obtain this response.

D. Saturation Functions

Saturation function is used instead of signum function to eliminate chattering. However the appropriate width of the function needs to be set. Smaller width means a faster response with higher possibility of chattering while larger width means the opposite. Here, $\phi = 50$ is chosen. This value doesn't cause chattering with an acceptable response speed.

Other parameters are listed in Table 3.1:

Table 3-1. Simulation Parameter

Simulation Data		
Sphere radius	r	300μm
Blood viscosity	η	5×10^{-3} Pa.s
Blood's density	ρ_f	1060 $kg.m^{-3}$
Bead's density	ρ_{sphere}	8000 $kg.m^{-3}$
Magnetization	M	1.950×10^{6} $A.m^{-1}$
Input saturation	u_{max}	$50mT.m^{-1}$
Blood velocity	v_f	$0.045+0.55\sin 2\pi t$
Time delay	L	0.002
Desired linear dynamics	K_D, K_P	20, 100

3.1.5. CONTROLLER TARGET

Despite the disturbance from the blood flow or noise from the sensor, the controller has to be able to control the movement of the microrobot to follow the trajectory. To determine the acceptable maximum error value, the environment and the microrobot size need to be considered. The blood vessel inner diameter is assumed to be 2mm and the microrobot has radius 0.3mm. As the microrobot is moved along the center line, it is required to keep the position error less than 0.7mm to avoid collision with the wall.

3.2. ACCURACY AND ROBUSTNESS EVALUATION

The proposed controller is an integration between time delay control (TDC) and terminal sliding mode (TSM). TDC uses time delay estimation to eliminate nonlinearities which offers a model-free control and TSM provide fast convergence to improve tracking accuracy. Thus it is expected for the proposed controller to be able to control the microrobot to move along the desired trajectory accurately while maintaining its robustness.

There are scenarios to be taken to evaluate the controller. To check the accuracy, the plant is kept simple. No disturbances except one from blood flow and no parameter variations are added into the simulation. This simulation shows how TDC can stabilize the system without prior knowledge of the plant. Then followed by the improvement by adding TSM into the controller.

For robustness evaluation, a disturbance force modeled as a step function is added. Also, a different value of blood viscosity is used. The controller performance is analyzed without changing controller gains. Here, how the controller perform without additional tuning and how much accuracy degrades are presented. Both scenarios don't include the actuator constraints and sensor noise.

Time Delay Control (TDC)

When TDC stands alone, $\bar{G}$ needs to be tuned to get the best result. Fig.3-4 shows the performance for three different $\bar{M}$: 0.001 (Fig.3-4a), 0.003 (Fig.3-4b), and 0.004 (Fig.3-4c). There are things in common. For all $\bar{G}$ value, there is always an undershoot at the beginning of the simulation. It happens because of the weight of the microrobot and the controller is not yet ready to lift it. The other thing is what seems like an oscillation when

the microrobot is suppose to be kept still. It is the result of the presence of the blood flow, which here is modeled as a sine wave.

When $\bar{M}$ is set to be 0.001, the undershoot is more than -3.6mm and the error caused by the flood flow is ranged from -1.27mm to 1.25mm. Increasing the $\bar{G}$ to 0.003 improves the performance. The undershoot is reduced to 1.23mm and the following error ranges from -0.37mm to 0.35mm. However, further increasing the $\bar{G}$ to 0.004 doesn't improve the result. Instead, it causes the control output sent to the actuator becomes very big, almost 100 times of the one with $\bar{G}$ = 0.001 or $\bar{G}$ = 0.003. Eventhough it's still trying to control the microrobot to follow the trajectory, the oscillation occurs which can lead to instability.

By seeing the result of TDC performance in Fig.3-4, it can be seen that TDC can stabilize the system even without prior knowledge of the plant. Nevertheless. the overall error is too big for the application. It is because an estimation error is inevitable due to a minimum limit of time delay one can use. Therefore, an additional term to the controller is required.

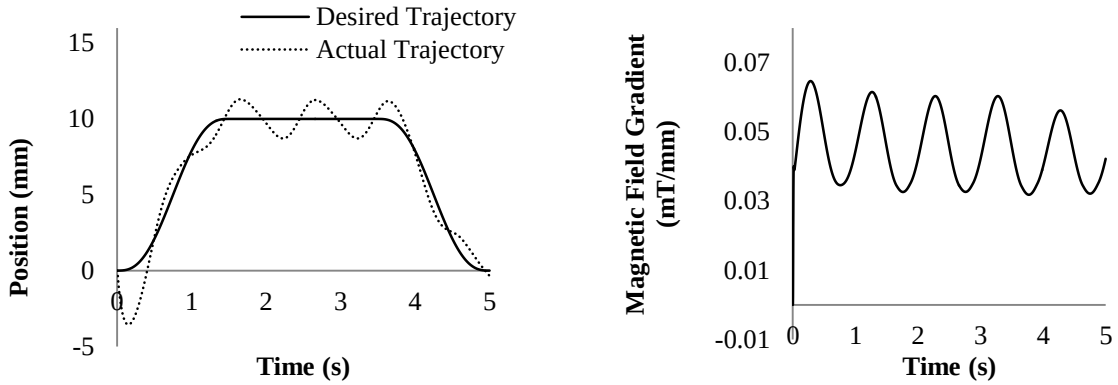

(a)

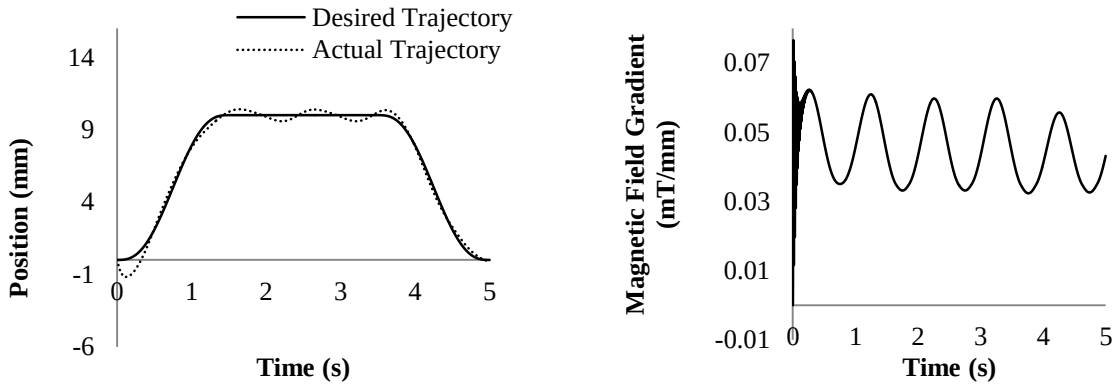

(b)

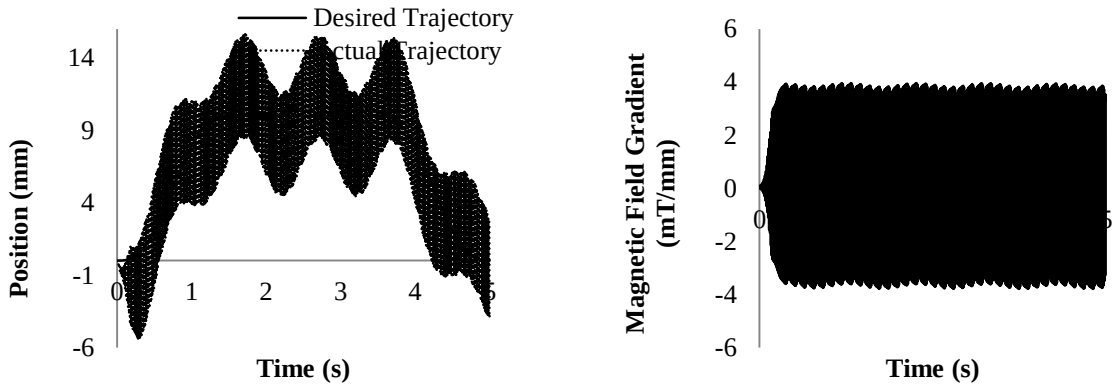

(c)

Figure 3-4. *Time Delay Control (TDC) Performance. Three different $\bar{G}$: (a) $\bar{G}$=0.001, (b) $\bar{G}$=0.003, and (c) $\bar{G}$=0.004. Left column is the trajectory graph. The desired trajectory is represented in solid line, and the actual trajectory is represented in dot line. Right column is the actuation. The actuation for $\bar{G}$=0.004 has different scale because it is far too big compared to the other two.*

Terminal Sliding Mode (TSM)

As mentioned before, TSM is supposed to improve the performance of the controller. Here, graphs shown are only the position error and the actuation. Position error is the difference between desired position and the actual position.

Adding TSM term into the controller gives two more constants to be tuned, K_{tsm} and γ. Together with $\bar{G}$, these three values determined the controller performance. The gain tuning is divided into two sets, the one with $\gamma = 0.6$ (Fig.3-5) and the one with $\gamma = 0.7$ (Fig.3-6). $\bar{G}$ is chosen from previous simulation minus $\bar{G} = 0.004$ due to its bad performance. To show how the controller works with small $\bar{G}$, additional value, $\bar{G} = 0.0005$ is added. Then, for each set of γ value and $\bar{G}$ value, K_{tsm} will be tuned to get the best result.

Increasing $\bar{G}$ or K_{tsm} or γ will reduce both overshoot and error. By observing Fig.3-5 and Fig.3-6, it can be seen that the three gain work side by side to obtain the best result. Nevertheless, there is a maximum value before the system becomes unstable. When $\bar{G}$ is increased, the freedom to change the other two gain becomes more constrained. While, if γ is set larger, K_{tsm} ranges becomes wider.

When $\bar{G}$ is set to be 0.003, one cannot make Ktsm too large and/or γ too small to keep it stable. However, when $\bar{G}$ is too small, the estimation error becomes larger and TSM must work harder to compensate it. As shown in Fig.3-5a ($\bar{G} = 0.0005$, $K_{tsm} = 200$, $\gamma = 0.6$), the overshoot is 0.38mm and the following error is -0.09mm to 0.07mm. In Fig.3-6a, ($\bar{G} = 0.0005$, $K_{tsm} = 300$, $\gamma = 0.7$), the overshoot is 0.36mm and the following error is from -0.1mm until 0.08mm. On the other hand, with actuation roughly similar for each counterpart, ones with $\bar{G}$ larger can obtain a better result. Fig.3-5b, ($\bar{G} = 0.001$, $K_{tsm} = 120$, $\gamma = 0.6$) shows a result with overshoot 0.28mm and the following error ranges from 0.076mm to 0.06mm. While Fig.3-6b, ($\bar{G} = 0.001$, $K_{tsm} = 150$, $\gamma = 0.7$), shows an overshoot 0.32mm and the error from -0.1mm until 0.08mm.

Overall, TSM addition to the controller greatly improves the controller. The result is satisfactory for the application. However, no unexpected disturbance added yet to the plant.

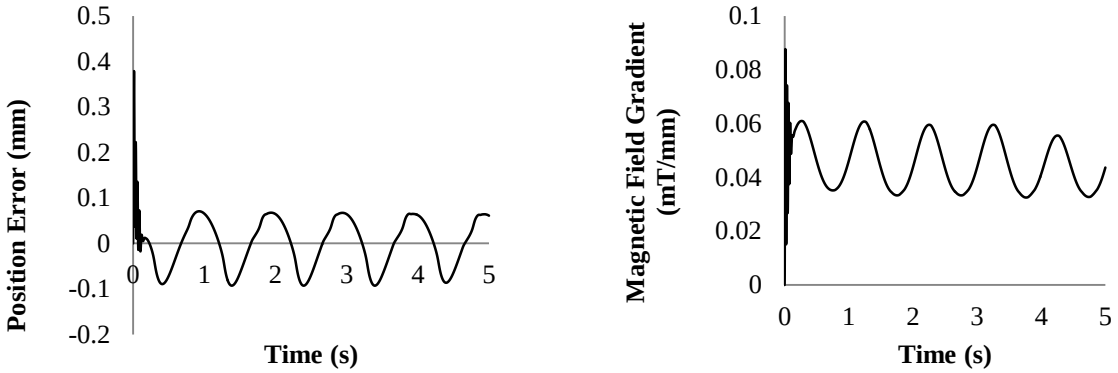

(a)

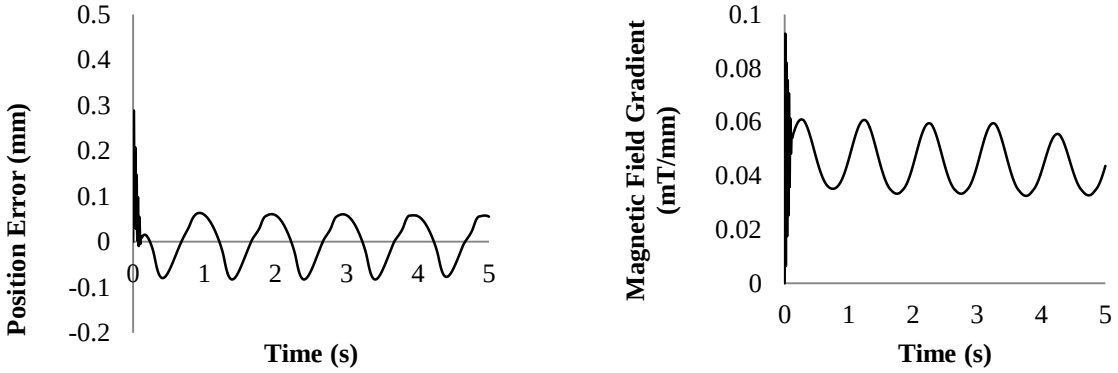

(b)

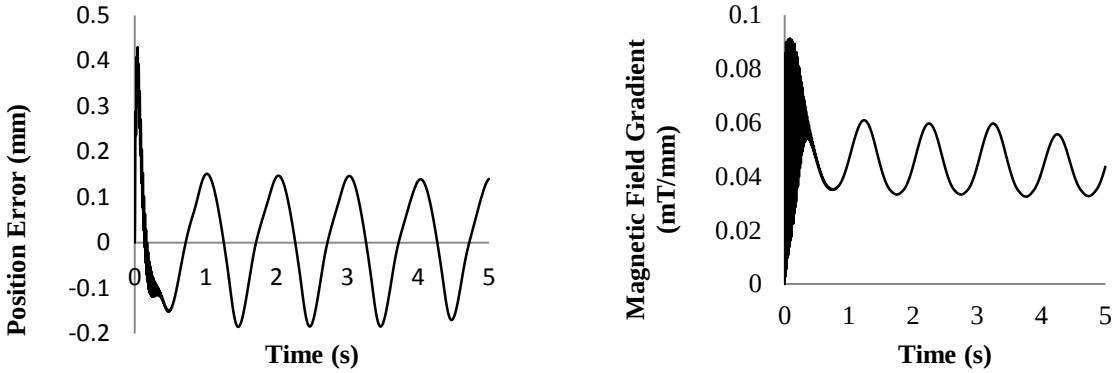

(c)

Figure 3-5. *Performance Improvement by Terminal Sliding Mode (TSM) with $\gamma = 0.6$. Three sets of controller gain: (a)$\bar{G} = 0.0005$, $K_{tsm} = 200$, (b) $\bar{G} = 0.001$, $K_{tsm} = 120$, and (c) $\bar{G} = 0.003$, $K_{tsm} = 10$. Left column is the position error which is the difference between the desired position and the actual position. It is in milimeter scale. Right column is the magnetic field gradient in mT/mm. Simulation time is 5s.*

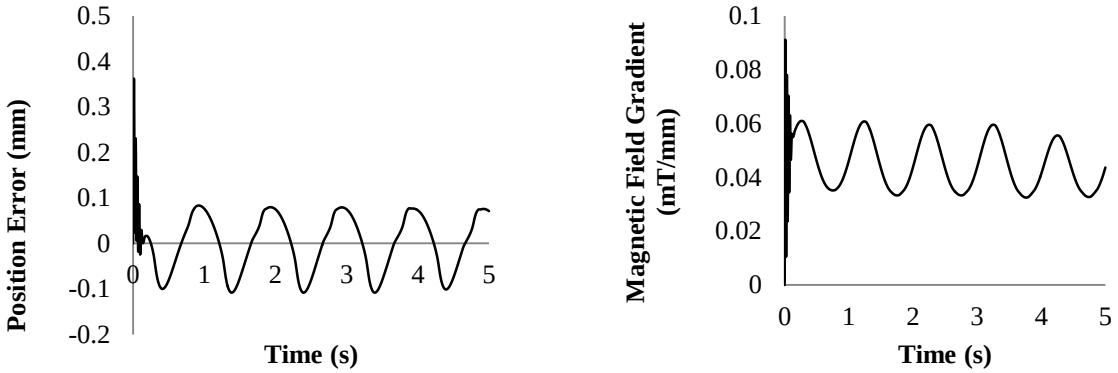

(a)

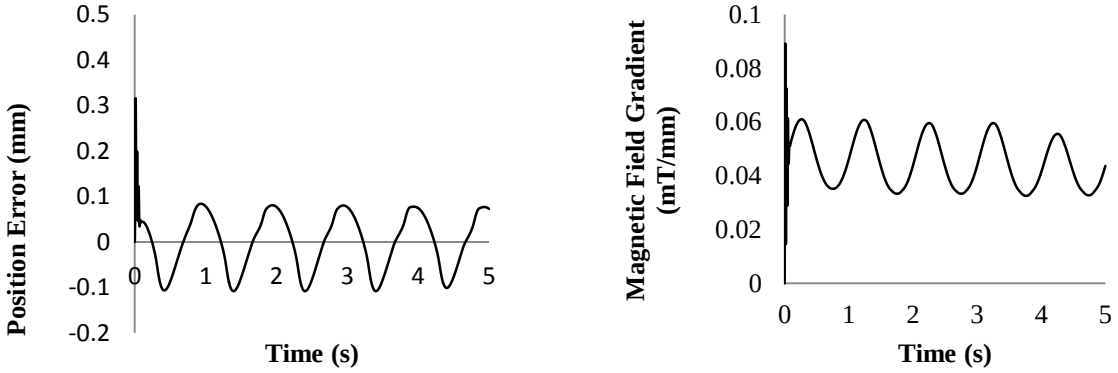

(b)

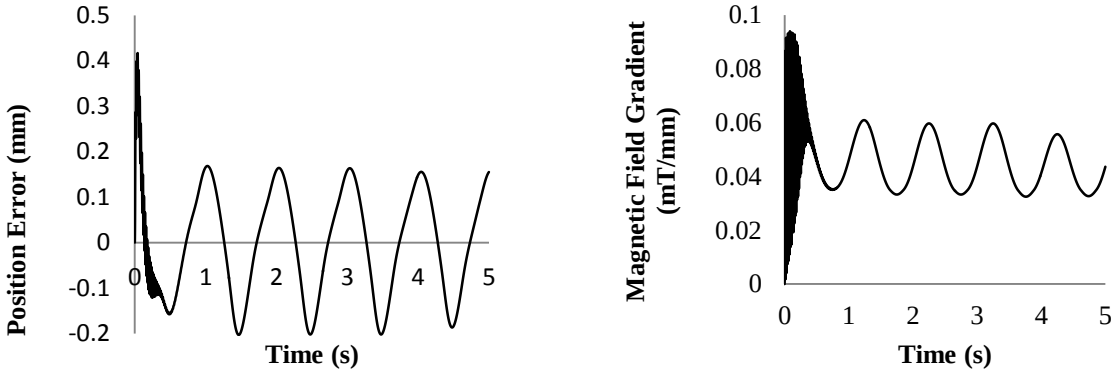

(c)

Figure 3-6. *Performance Improvement by Terminal Sliding Mode (TSM) with $\gamma = 0.7$. Three sets of controller gain: (a) $\bar{G} = 0.0005$, $K_{tsm} = 300$, (b) $\bar{G} = 0.001$, $K_{tsm} = 150$,and (c) $\bar{G} = 0.003$, $K_{tsm} = 15$. Left column is the position error in milimeter scale. Right column is the magnetic field gradient in mT/mm. Simulation time is 5s.*

Robustness Analysis

After previous simulation, it is decided that the best gain set would be $\bar{G}$ = 0.001, K_{tsm} = 120, γ = 0.6. Using this set, the robustness evaluation is conducted. There are three evaluations. First is when there is a different viscosity value, second is adding a disturbance force, and third is a combination of both. Robustness against noise will be done separately.

The viscosity used is $6x10^{-3}$ Pa.s which is 10^{-3} Pa.s larger than the previous value. The result is shown in Fig.3-7a. No changes happen both to the performance and the actuation. It shows that the proposed controller is robust against viscosity value variation.

On the other hand, when a disturbance force is added, there is a slightly degradation. The force is modeled as a step function with final value $2.5x10^{-6}$N starting from t = 1s. The value doesn't have physical meaning. It is chosen to be around 15% than other forces total amplitude calculated in (3-14). As can be seen in Fig.3-7b, a second overshoot is occured at the beginning of the disturbance. The similar result happens in Fig.2-7c when both scenarios are combined. The overshoot at t = 1s is 0.14mm. This value is still acceptable as it's still in the range of the controller target. However, the magnetic field gradient required to achieve the result is higher than before. This can lead to saturation problem which will be discussed in the next simulation.

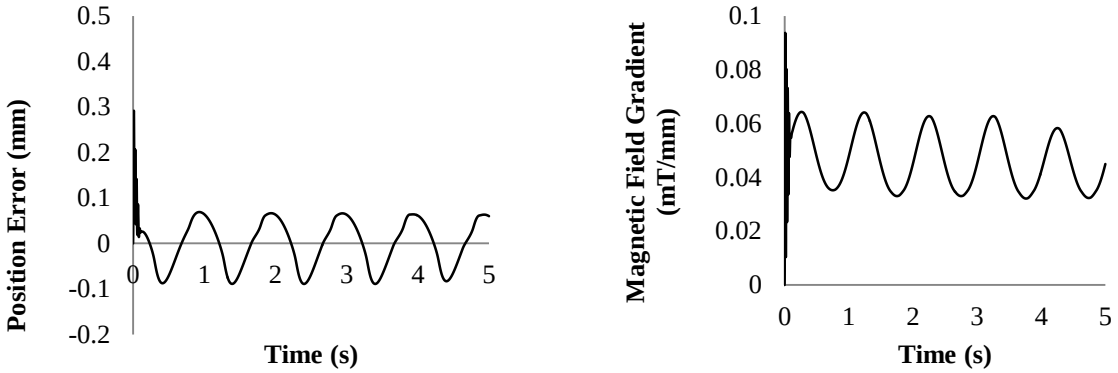

(a)

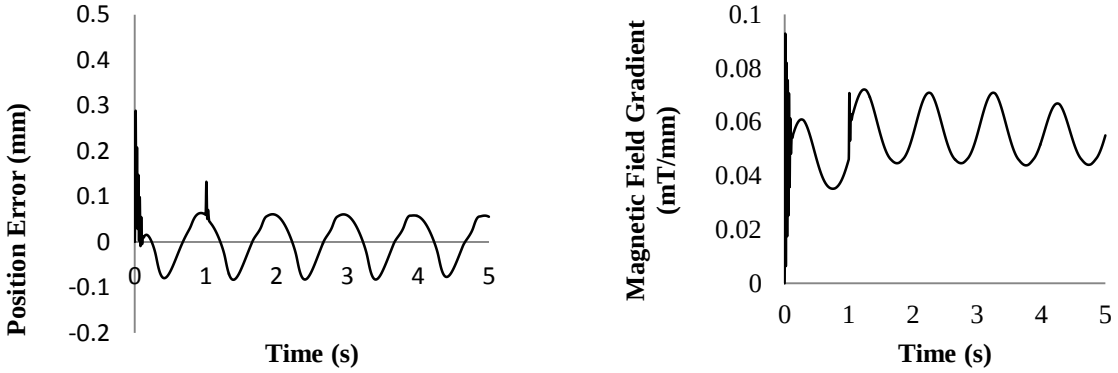

(b)

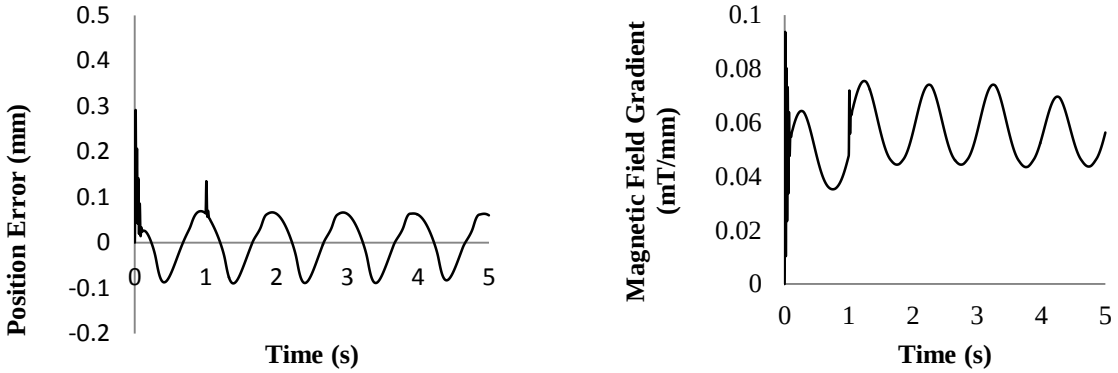

(c)

Figure 3-7. *Robustness Evaluation. (a) Parameter variation in blood viscosity. It is set equal to $6x10^{-3}$ Pa.s (b) A disturbance force with value 10^{-6} at $t \geq 1s$. (c) A combination of parameter variation and disturbance force. Left side is for position error in milimeter scale. Right side is for magnetic field gradient in mT/mm. The simulation is done in 5s.*

3.3. ANTI-WINDUP SCHEME EVALUATION

An actuator has an upper limit for how much power it can provide. This limit is added to the simulation. After a calculation done in (3-14) and (3-15), it is expected that the system won't reach saturation. However, as the proposed controller combines TDC and TSM, there are two integration involved. These integration can cause a windup effect that leads to a saturation.

Fig.3-8 gives the result when disturbance is not included. Because the limit is set larger enough than the required field gradient, even if the windup effect is occured, it doesn't give any problem. As there are no saturation, anti-windup scheme performance cannot be evaluated here. Meanwhile, when a disturbance is involved, a saturation occured. Fig.3-9 shows the trajectory graph when the plant is affected by a disturbance with the controller is assisted with the anti windup. Here there are some big error at some position. By calculating the required gradient field, after adding a disturbance, it turns out it exceeds the actuator limit. However it serves the simulation purpose to evaluate the scheme as the actuator will certainly be saturated. The calculation for the required gradient when a disturbance force is applied to the plant is as followed:

$$F_{m_{min}} = |W_a + F_D + d| = (7.69 + 6.32 + 2.5) \times 10^{-6} = 16.5 \times 10^{-6} N \quad (3\text{-}16)$$

$$\nabla B_{min} = \frac{F_{m_{min}}}{(M \times V)} = 0.075\ T/m \quad (3\text{-}17)$$

Fig.3-10 shows the effectiveness of anti-windup schemes. In Fig.3-10a, the scheme has not yet added and the saturation is occured for a long time as the undershoot reaches almost 2mm. After adding anti-windup for TDC (Fig.3-10b), the saturation duration is reduced and so the undershoot is also reduced to 0.37mm. After adding anti-windup for TSM (Fig.3-10c), the undershoot is further reduced to none.

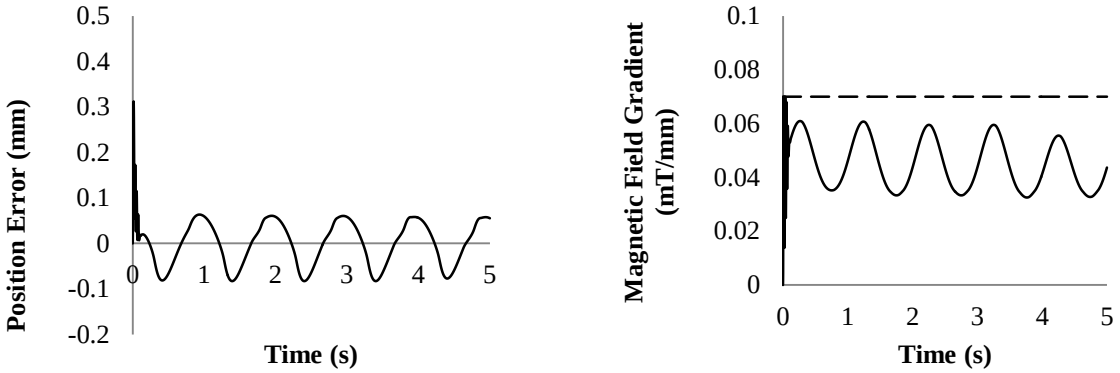

Figure 3-8. *Controller Performance with Actuator Constraints. The limit of the actuator is 70mT/mm as represented by black dash line in the magnetic field gradient graph. No disturbance is added. Right side is the position error in milimeter and left side is the field gradient in mT/mm.*

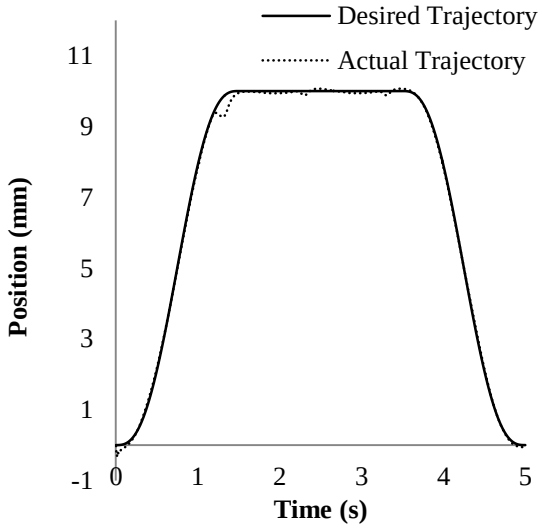

Figure 3-9. *The Trajectory for A Microrobot with Disturbance. Solid line is the desired trajectory and dot line is the actual trajectory. The y-axis represents position in milimeter and the x-axis represents time in seconds. The disturbance force is 2.5x10-6N. Anti-windup for both TDC and TSM are added. Gain for TSM anti-windup is 30.*

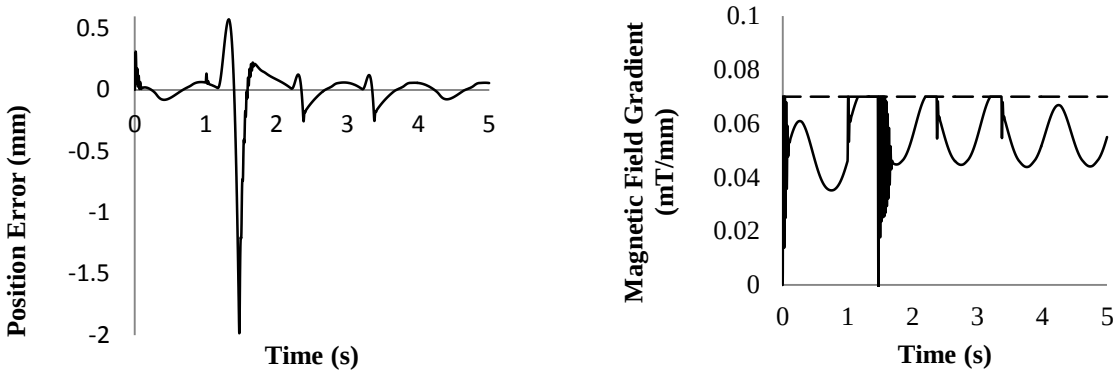

(a)

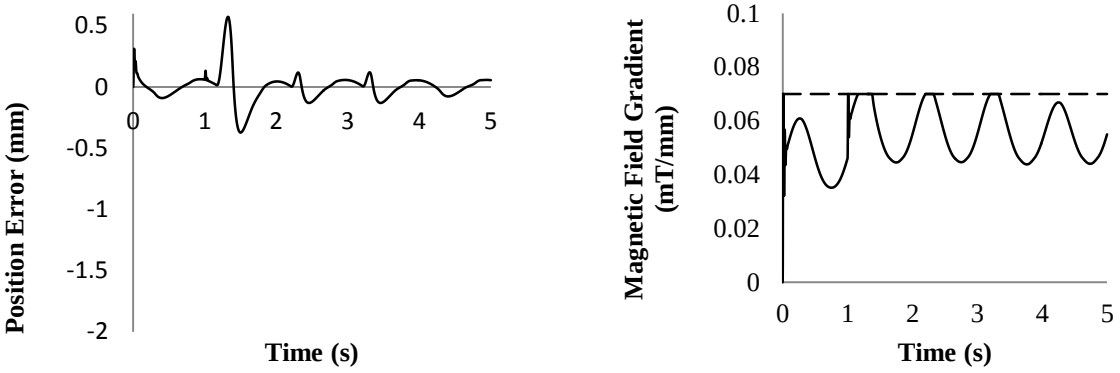

(b)

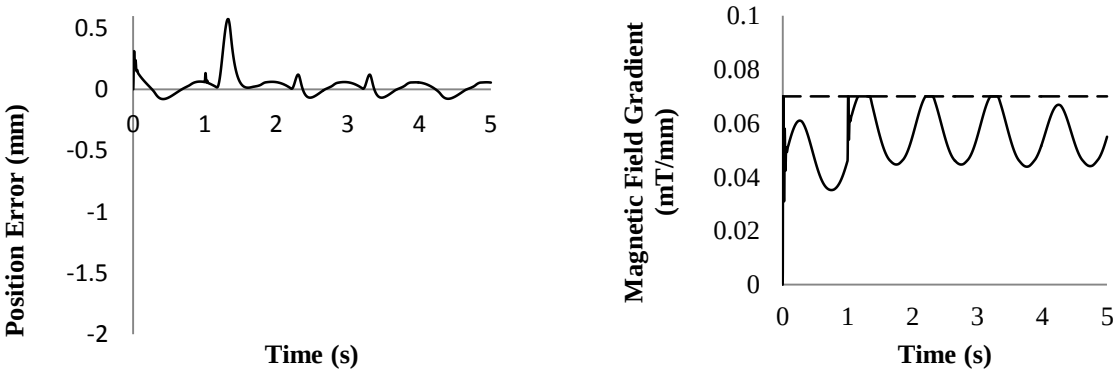

(c)

Figure 3-10. *Anti-Windup Scheme Evaluation. (a) No anti-windup, (b) Anti-windup for TDC is added, and (c) Anti-windup for both TDC and TSM are added. Left side is position error in milimeter and right is magnetic field gradient in mT/mm. The black dash line (--) represents the limit of the actuator (u_{max} = 0.07mT/mm).*

3.4. SOLUTION FOR MEASUREMENT NOISE

A sensor is inevitably not perfect. The problem comes as the proposed controller requires velocity and accelaration information which are obtained by using numerical differentiation. This makes, no matter small an error in position measurement, it becomes larger in velocity and acceleration region depending on the size of sampling time. However, this sampling time is equal to time delay in TDE. Therefore there is a trade between the accuracy of TDE and the robustness against noise.

Fig.3-11 to Fig.3-18 show how the controller performs with noise present. The measurement noise is modeled as a random number with maximum/minimum value ±0.1mm. Two solutions are compared. First is by lowering the controller gain and second is by using a low pass filter.

Solution 1: Lowering Gain Value

Without TSM, TDC needs to lower $\bar{G}$ to keep the system stable. Here, $\bar{G}$ used is 0.0005. This results a very big error in returns as shown in Fig.3-11. Meanwhile, Fig.3-12 shows the proposed controller performance against noise. To see how it works, there are three gain sets to compare. For every set, γ value is kept constant to simplify the tuning and the analysis. While for $\bar{G}$ value, two different values are used, 0.0002 and 0.0003. Both are smaller than the value from previous simulation (Fig.3-11) to reduce the effect of the explosion of acceleration term in TDC controller.

Fig.3-12a ($\bar{G}$ = 0.0002, K_{tsm} = 250, γ = 0.6) shows an overshoot at 0.9mm and error ripples with minimum value at -0.28mm and maximum value at 0.29mm. Fig.3-12b ($\bar{G}$ = 0.0002, K_{tsm} = 370, γ = 0.6) shows a better overshoot result which is 0.66mm with a worse following error. The ripple is more severe with values ranges from -0.29mm to 0.44mm. In Fig.3-12c ($\bar{G}$ = 0.0003, K_{tsm} = 150, γ = 0.6), the overshoot is 0.92mm and the error ripples from -0.25mm to 0.38mm.

Compared to Fig.3-11, Fig.3-12 shows a much better results. After TSM is added, as there are other gain can be tuned beside $\bar{G}$, the outcome can be controlled more freely. Also, because the sliding manifold of the TSM doesn't require acceleration information, it makes TSM slightly unaffected compared to TDC. This shows that TSM term adds the robustness against noise to the overall controller.

The controller target is to keep the error less than 0.7mm. From the simulation, the second gain set for the proposed controller gives an overall error performance which satisfies the criteria. Even though it has more ripple compared to other sets of gain, the maximum/minimum value doesn't exceed the application requirement.

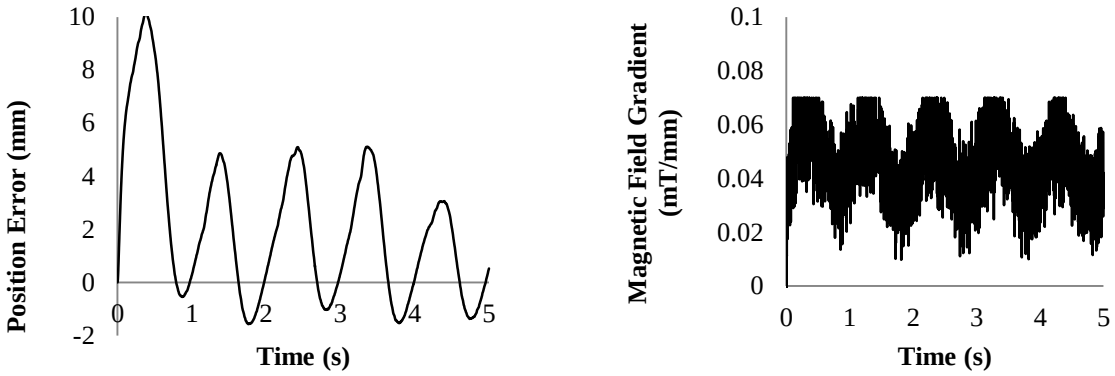

Figure 3-11. *TDC Performance with Noise Present. Noise is random numbers with max/min value = ±0.1mm. Controller gain $\bar{G}$ = 0.0005. Left side is position error in milimeter and right side is magnetic field gradient in mT/mm*

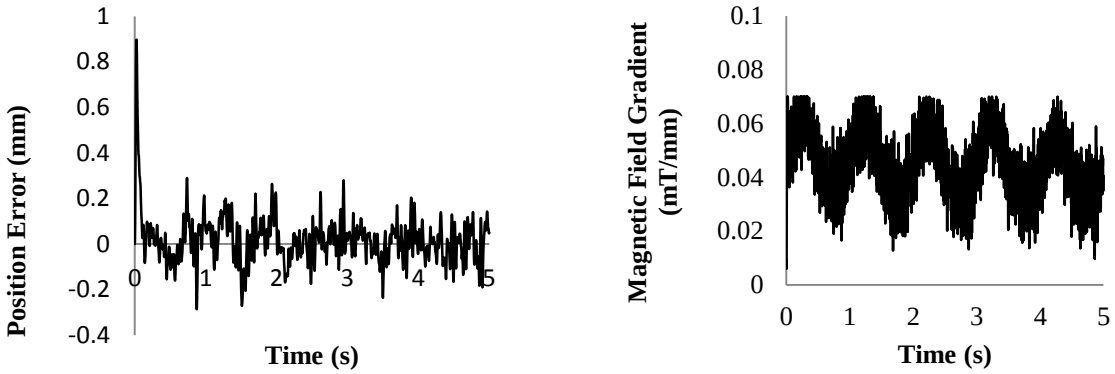

(a)

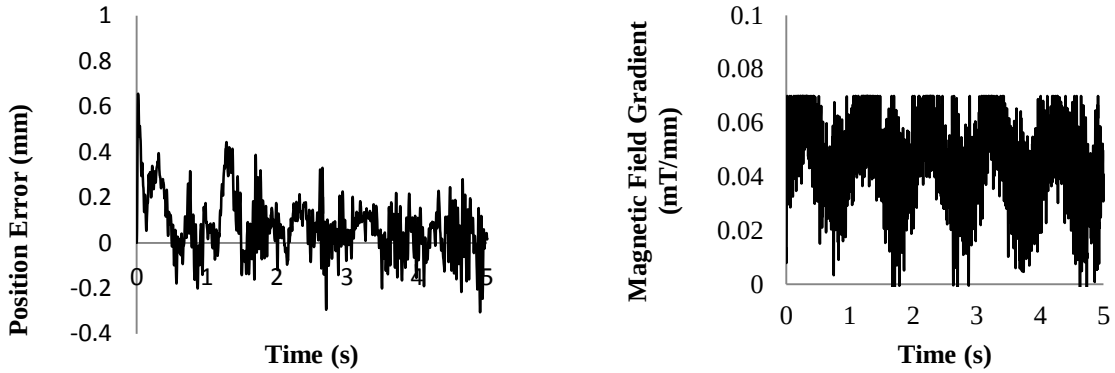

(b)

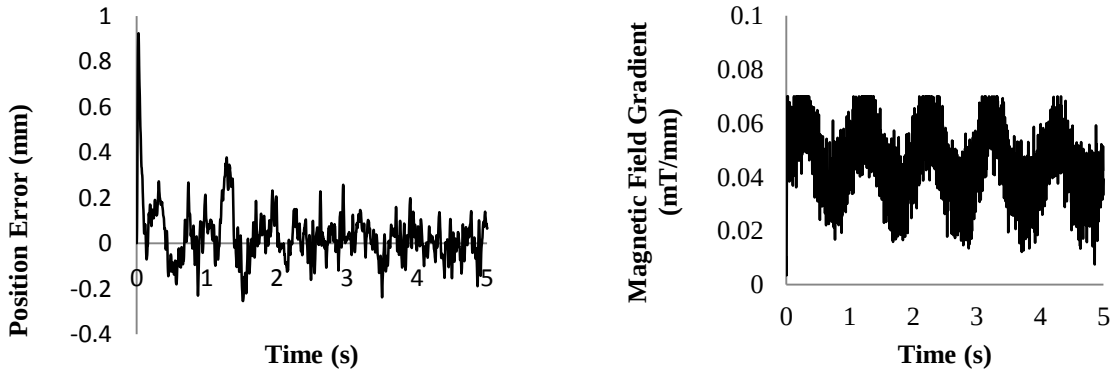

(c)

Figure 3-12. *Proposed Controller Performance with Noise Present. Noise is random numbers with max/min value = ±0.1mm. There are three different sets of gain: (a) $\bar{G}$ = 0.0002, K_{tsm} = 250, γ = 0.6 (b) $\bar{G}$ = 0.0002, K_{tsm} = 370, γ = 0.6, and (c) $\bar{G}$ = 0.0003, K_{tsm} = 150, γ = 0.6. Left side is position error in milimeter and right side is magnetic field gradient in mT/mm*

Solution 2: Adding Low Pass Filter (LPF)

Previous solution gives a good tracking performance, but there is a chattering in the actuation. It may cause overheating to the actuator. LPF is able to smooth the signal and reduce the noise amplitude. It is expected that the filter can smooth the control command. Also, by adding a filter term, $\overline{G}$ value choices can be wider that it may improve the tracking performance. The simulation compares between placements of the filter. Here, time constant is kept the same, that is $\tau = 0.01$. After the best place is selected, three different time constants are compared.

The location of the LPF is divided into whether it is installed separately from the controller or integrated:

- External Filter

External filter means that it is placed outside of the controller. There are two location here to be compared as shown in Fig.3-13. First is between the sensor and the controller. It smooths the signal feeding the controller. Meanwhile, the second filter location smooths the noise or chattering in the output signal sent to the actuator.

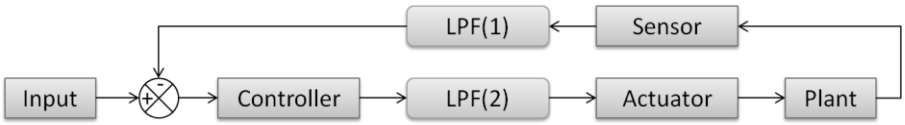

***Figure 3-13**. External Filter Placement. Two locations represented in orange-colored block.*

Same as previous simulations, the proposed controller is compared with TDC to see how the additional TSM term gives improvement into the controller. Fig.3-14 is for TDC and Fig.3-15 is for the proposed controller. Fig.3-14a and Fig.3-15a shows the controller performance for when the filter is put in the location 1. While Fig.3-14b and Fig.3-15b is for when the filter is in location 2. Placing the filter in location 1 shows a worse result. While measurement noise does degrade the derivative action which leads to chattering in the control output, this effect is not very concerning for proportional action. Moreover, integral action is unaffected by noise because the constant summing of error literally averages the random variations in the signal. Since filtering adds delay and this hurts best possible control performance, and because noise is not an issue for proportional and integral action, this location is not the best for filtering.

In the end, adding TSM term may improve the performance. However, for overall result in this simulation, putting filter at both location causes a worse performance compared to ones without additional filter (Fig.3-12). Therefore, another location for filter is tried in the next simulation.

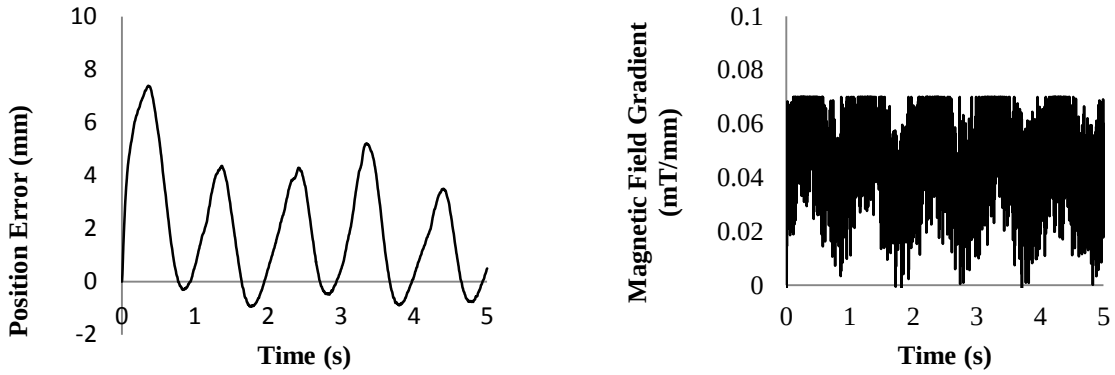

(a)

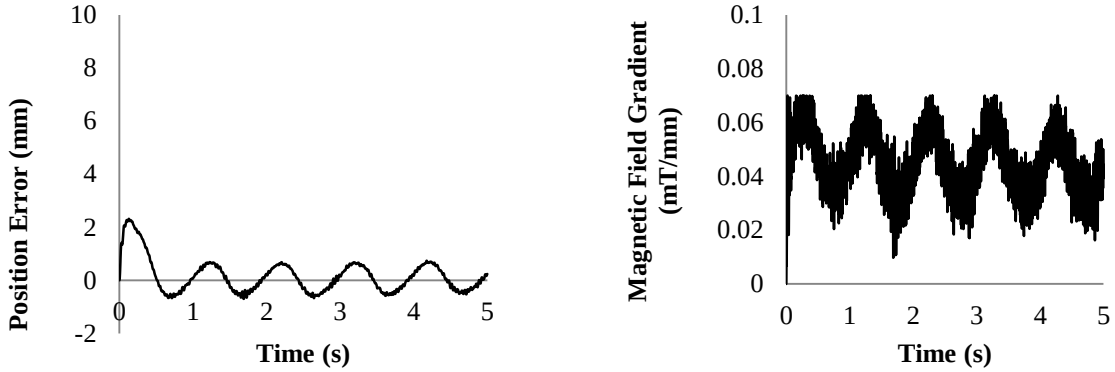

(b)

Figure 3-14. *TDC with External LPF Performance Against Noise. Noise is a random number with max/min value = ±0.1mm. (a) $\bar{G}$ = 0.002. LPF is placed in location 1: to filter the feedback position. (b) $\bar{G}$ = 0.004. LPF is placed in location 2: to filter the control output.*

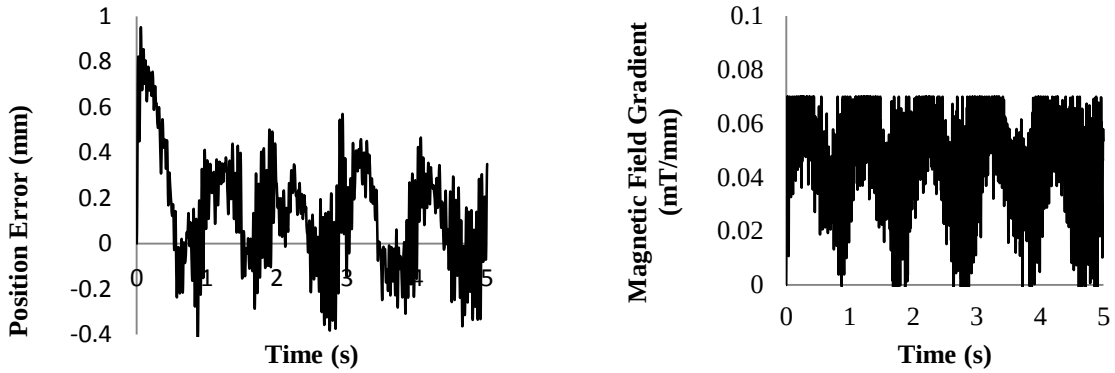

(a)

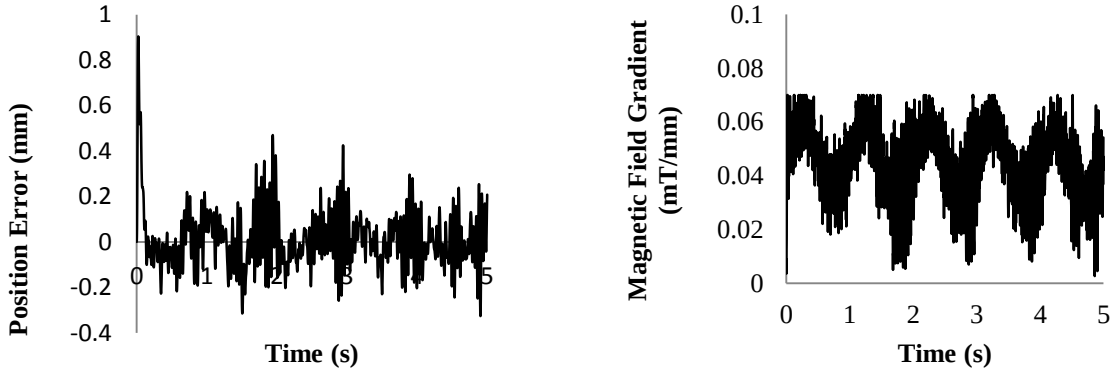

(b)

Figure 3-15. *The Proposed Controller (TDC + TSM) with External LPF Performance Against Noise. Noise is a random number with max/min value = ±0.1mm. (a)* $\bar{G}$ *= 0.001,* K_{tsm} *= 400,* γ *= 0.6. LPF is placed in location 1: to filter the feedback position. (b)* $\bar{G}$ *= 0.0005,* K_{tsm} *= 100,* γ *= 0.6. LPF is placed in location 2: to filter the control output.*

- Internal Filter

For feedback control, filtering need only be applied to the signal feeding the derivative term. As stated before, noise does not present a problem for proportional and integral action. These elements will perform best without the delay introduced from a signal filter.

Here, instead of using numerical differentiation (2-32, 2-33) , a first order low pass filter is used to obtain the velocity and the acceleration information with equation as follows

$$\dot{y} \approx \dot{y_{filt}} = \frac{1}{\tau}\left(-y_{filt} + y\right) \tag{3-18}$$

where y is the filter input and y_{filt} is the filtered signal.

Fig.3-16 is for TDC which use ($\bar{G}$ = 0.002) and Fig.3-17 is for the proposed controller ($\bar{G}$ = *0.0005*, K_{tsm} = *100*, γ = *0.6*). In case of the filter location, there are two place will be compared. First, filter is used to calculate the velocity (Fig.3-16a and Fig.3-17a) and second, to calculate the acceleration (Fig.3-16b and Fig.3-17b).

As to be expected, the proposed controller is better than TDC. When integral filter is used for calculating velocity (Fig.3-17a), the overshoot is 0.66mm and the following error ranges from -0.3mm to 0.5mm. While when filter is used for calculating acceleration (Fig.3-17b), the overshoot is 0.65mm and the following ranges from -0.3mm to 0.5mm. Both gives the same performance in terms of position error. The similarity also can be seen in the control effort.

The error in this simulation shows a relatively small overshoot with a big ripple. The result is somewhat similar to the one without filter (Fig.3-12b). However, the gain tuning has more freedom compared to the controller without filter. Therefore, next simulation will be about finding the best filter time constant to see whether it can more improve the performance.

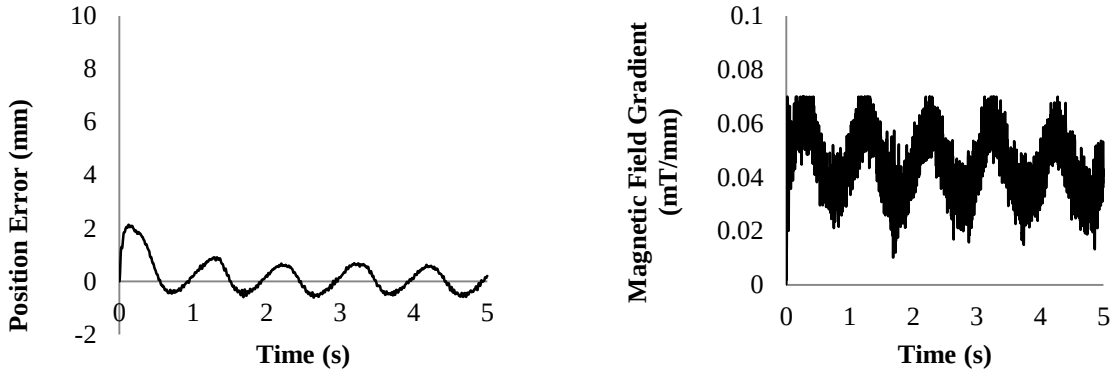

(a)

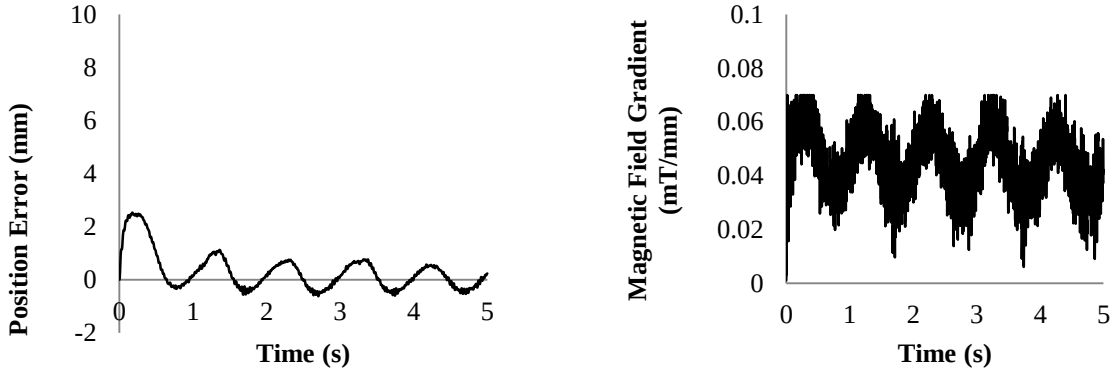

(b)

Figure 3-16. *TDC with Internal LPF Performance Against Noise. Noise is a random number with max/min value = ±0.1mm.* $\bar{G}$ *= 0.002. (a) LPF is used to calculate velocity. (b) LPF is used to calculate acceleration.*

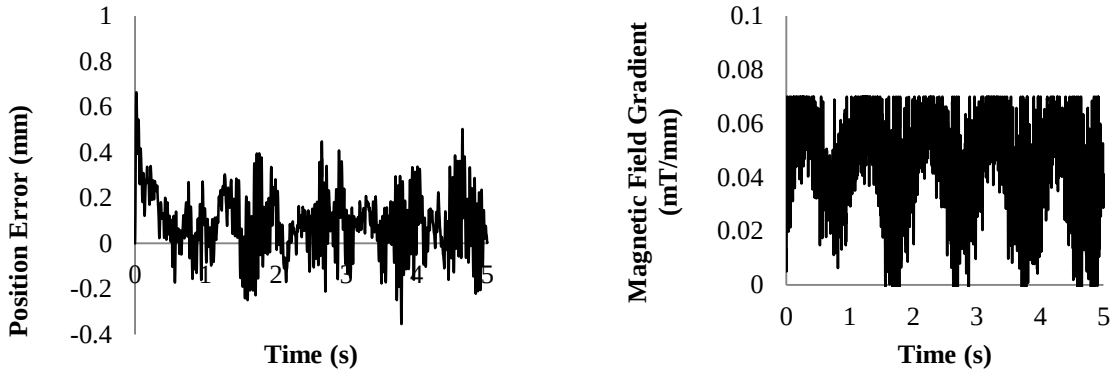

(a)

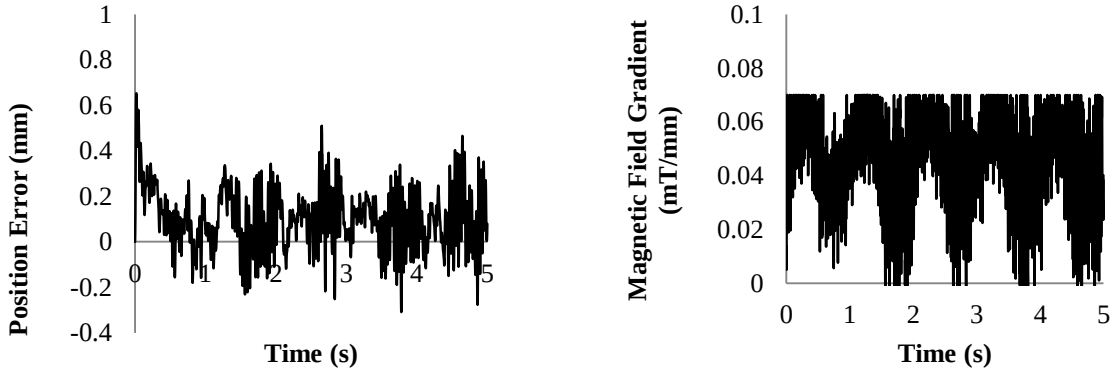

(b)

Figure 3-17. *The Proposed Controller (TDC + TSM) with Internal LPF Performance Against Noise. Noise is a random number with max/min value = ±0.1mm.* $\bar{G}$ *= 0.0005,* K_{tsm} *= 150,* γ *= 0.6. (a) LPF is used to calculate velocity. (b) LPF is used to calculate acceleration.*

Next simulation is to see how the time constant of the filter influence the error and the actuation performance. As known, a bigger time constant means smoother output with bigger phase shift. For comparison, there are three time constants (τ = 0.1, 0.05, 0.005) will be simulated with same controller gain set ($\bar{G}$ = *0.0005*, K_{tsm} = *150*, γ = *0.6*). The filter location and gain values are chosen similar as the previous simulation shown in Fig.3-17b.

By seeing Fig.3-18, increasing time constant may degrades the error performance. The overshoot is similar for all three value, around 0.65mm. The difference is in the ripple. As time constant increased, the ripple becomes more frequent. As shown, for same gain set, the best result is the controller with filter with the least time constant, τ = 0.005 (Fig.3-18c). The error after the overshoot ranges from -0.25mm to 0.48mm.

Unfortunately, after changing the filter cutoff frequency, the result still doesn't improve. It has the same performance with the first noise solution, which is by lowering gain value. However, this solution is worse due to an additional constant to be tuned.

Adding a low pass filter allows the $\bar{G}$ to be tuned bigger. However, a bigger $\bar{G}$ value means a stricter TSM gain selection. As the noise results a chattering in the control output signal, it tends to force the actuator to reach saturation faster. Therefore, there is a limit of error performance the controller can achieve.

The design challenge is to find the careful balance between signal smoothing and information delay to achieve the controller performance we desire for our application. A "better" filter design is one that decreases the random variation while retaining more of the true dynamic information of the original signal. And, using a simple first order low pass filter doesn't fit the criteria. That is why it doesn't give any improvement.

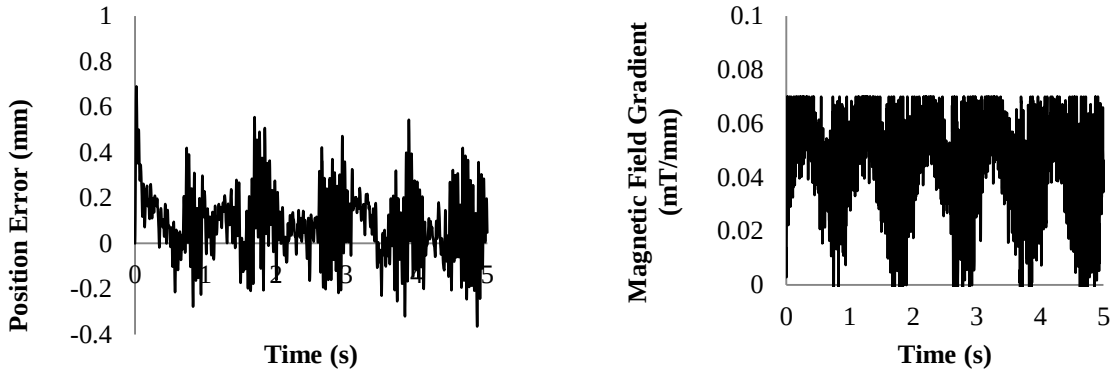

(a)

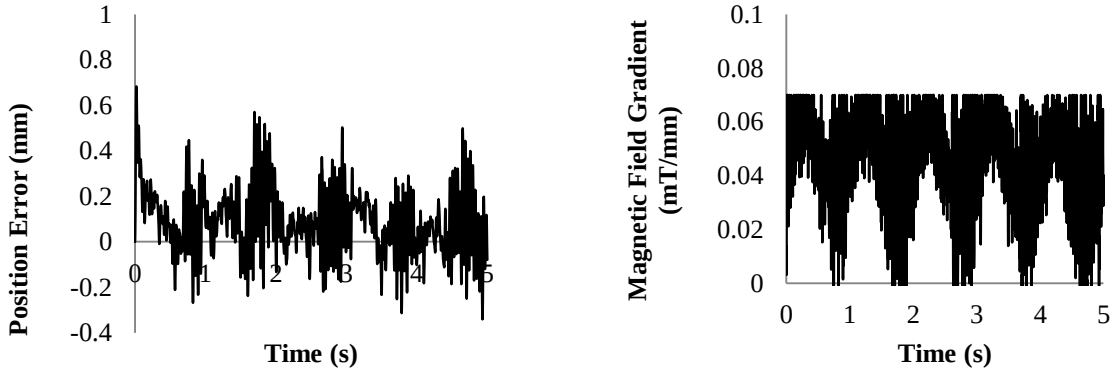

(b)

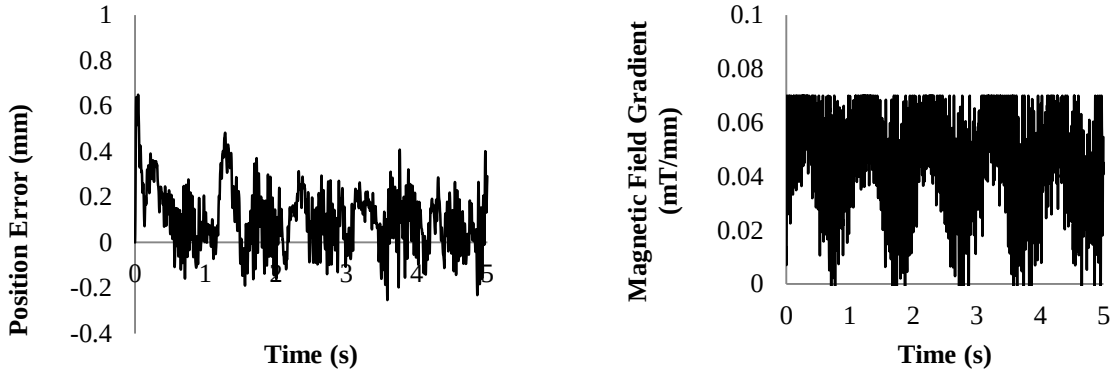

(c)

Figure 3-18. *Comparison of Controller Performance with Different Filter Time Constant. The LPF is used to calculate acceleration. Controller gain:* $\bar{G}$ *= 0.0005,* K_{tsm} *= 150,* γ *= 0.6. (a)* τ *= 0.1, (b)* τ *= 0.05, and (c)* τ *= 0.005.*

3.5. 2 DIMENSION

Previous simulations only consider the microrobot to move in one dimension, that is Z-axis. Here, the microrobot will be simulated to move on two dimension. It will move up 45^o on the XZ-plane along the centerline of the blood vessel. The simulation will be 1.5s. There are 3 conditions in these simulations which are when the drag force value is increased 20% from previous simulation, when there is a measurement noise, and last is when both situations are present. Sensor accuracy is set the same as previous simulation, that is 0.1mm. Lowering gain value is chosen as the solution for the noise.

The position error graph will be calculated by using the following equation:

$$e = \sqrt{(x_d + x)^2 + (z_d + z)^2} \tag{3-19}$$

Best tuned controller gains sets from previous simulation are used to show that the proposed controller doesn't need additional tuning. When there is no measurement noise controller gains are set $\bar{G}$ = 0.001, K_{tsm} = 120, and γ = 0.6. While when there is a measurement noise, controller gains are set $\bar{G}$ = 0.0002, K_{tsm} = 370, and γ = 0.6.

The actual trajectory is being compared with the desired trajectory. Here, whether the microrobot will collide to the wall is also checked. For that, the microrobot is modeled as circle is drawn on the biggest position error. From Fig.3-19a and Fig 3-19b, eventhough there is no additional tuning, when the drag force is 20% bigger, the controller can maintain its performance. The microrobot doesn't collide to the wall and the tracking performance doesn't not significantly degrade.

When the measurement noise is present, looking slightly to the trajectory graph in Fig.3-19d, the actual trajectory is somewhat overlapping with the desired trajectory. However, if one sees it closer, the microrobot is moving back and forth to reach the desired position with the biggest error reaches 0.6mm. By observing the field gradient graph, it can be seen that the actuator reaches saturation a few times. That is why the microrobot keeps getting pushed at. This result are similar to when both situations are applied to the simulation.

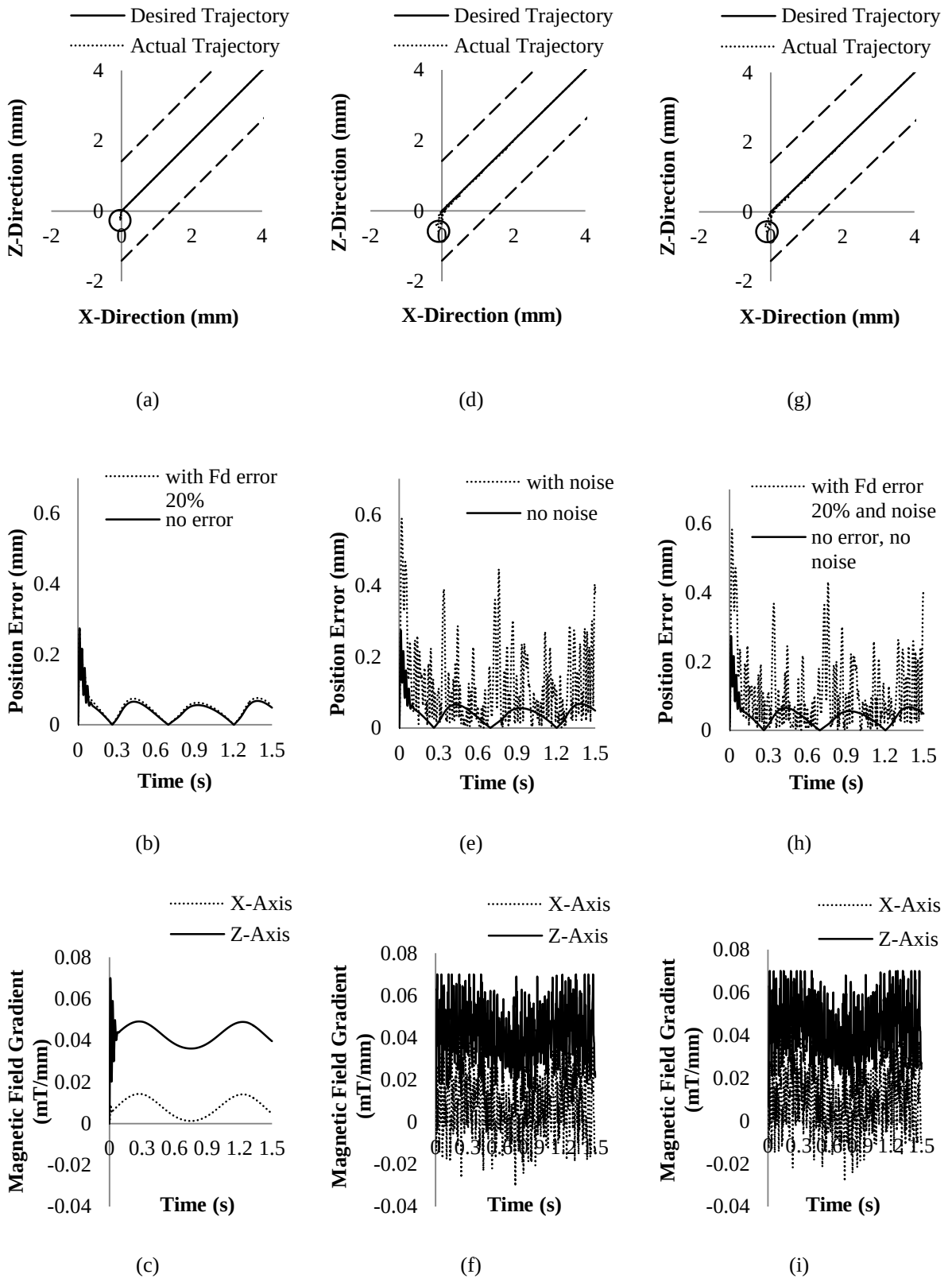

Figure 3-19. *Simulation for A Microrobot Moving on An XZ-Plane. First row is the trajectory graph (a,d,g) with solid line represents desired trajectory and dot line represents the actual trajectory. Dash lines is the vessel walls and the circle is the microrobot with radius 0.3mm. The second row is the position error graph (b,e,h). Solid line is when uncertainties are included and dot line is when they are not. The third row is the field*

gradient graph (c,f,i). Dot line is the actuation for X-axis and solid line is the actuation for Z-axis. (a-c) The drag force is 20% bigger than when the controller gain is being tuned. Controller gains are $\bar{G}$ *= 0.001,* K_{tsm} *= 120, and* γ *= 0.6. (d-f) Measurement noise is present with sensor accuracy despite noise is 0.1mm. Controller gains are* $\bar{G}$ *= 0.0002,* K_{tsm} *= 370, and* γ *= 0.6. (g-i) Both drag force value difference and noise are present. Controller gains are* $\bar{G}$ *= 0.0002,* K_{tsm} *= 370, and* γ *= 0.6.*

CONCLUSION AND FUTURE WORKS

CONCLUSION

In this thesis, a scheme has been built to control a microrobot to move in a blood vessel by following a predetermined trajectory safely and accurately. It combines time delay control (TDC) and terminal sliding mode (TSM) control. TDC allows a model-free control as it eliminates uncertainties and injects the desired dynamics while TSM works to reduce TDC estimation error. Anti-windup scheme also included in the controller to avoid windup phenomenon.

Simulations have been conducted to evaluate the accuracy and the robustness of the proposed controller. For that, a real condition is considered in simulations, such as presences of actuator saturation and measurement noise. After simulations, the proposed controller is proven to be accurate and robust against disturbance and parameter variations. Anti-windup schemes integrated to the controller are also proved to be able to eliminate accumulated error. Meanwhile, when the feedback signal is affected by noise, the performance degrades. Eventhough, the tracking performance is still satisfactory to the controller target, the controller output is chattering. A real actuator system may not be able to provide the required field gradient. Also, it may cause overheating.

FUTURE WORKS

A controller improvement needs to be made especially in the presence of measurement noise. Therefore the future research is focusing on how to refine the control output while keeping the tracking performance or even better improving it. More simulations are also needed with a more complex plant model and more constraint in the actuator to further confirm that the proposed controller is accepted to be applied to a real system. After all simulation conditions are fulfilled, an experiment will be conducted.

REFERENCES

1. Nelson, B.J., I.K. Kaliakatsos, and J.J. Abbott, *Microrobots for Minimally Invasive Medicine.* Annual Review of Biomedical Engineering, Vol 12, 2010. **12**: p. 55-85.
2. Huaming, L., T. Jindong, and Z. Mingjun, *Dynamics Modeling and Analysis of a Swimming Microrobot for Controlled Drug Delivery.* Automation Science and Engineering, IEEE Transactions on, 2009. **6**(2): p. 220-227.
3. Arcese, L., M. Fruchard, and A. Ferreira, *Endovascular Magnetically Guided Robots: Navigation Modeling and Optimization.* Biomedical Engineering, IEEE Transactions on, 2012. **59**(4): p. 977-987.
4. Ishiyama, K., M. Sendoh, and K.I. Arai, *Magnetic micromachines for medical applications.* Journal of Magnetism and Magnetic Materials, 2002. **242–245, Part 1**(0): p. 41-46.
5. Mathieu, J.-B., G. Beaudoin, and S. Martel, *Method of propulsion of a ferromagnetic core in the cardiovascular system through magnetic gradients generated by an MRI system.* Biomedical Engineering, IEEE Transactions on, 2006. **53**(2): p. 292-299.
6. Mathieu, J.B., et al. *Preliminary studies for using magnetic resonance imaging systems as a mean of propulsion for microrobots in blood vessels and evaluation of ferromagnetic artefacts*. in *Electrical and Computer Engineering, 2003. IEEE CCECE 2003. Canadian Conference on*. 2003.
7. Tamaz, S. and S. Martel. *Impact of the MRI-based Navigation System Constraints on the Step Response Using a PID Controller*. in *Engineering in Medicine and Biology Society, 2005. IEEE-EMBS 2005. 27th Annual International Conference of the*. 2005.
8. Arcese, L., et al. *High Gain Observer for backstepping control of a MRI-guided therapeutic microrobot in blood vessels*. in *Biomedical Robotics and Biomechatronics (BioRob), 2010 3rd IEEE RAS and EMBS International Conference on*. 2010.
9. Arcese, L., et al. *Adaptive backstepping and MEMS force sensor for an MRI-guided microrobot in the vasculature*. in *Robotics and Automation (ICRA), 2011 IEEE International Conference on*. 2011.
10. Arcese, L., M. Fruchard, and A. Ferreira, *Adaptive Controller and Observer for a Magnetic Microrobot.* Robotics, IEEE Transactions on, 2013. **PP**(99): p. 1-8.
11. Youcef-Toumi, K. and O. Ito. *A Time Delay Controller for Systems with Unknown Dynamics*. in *American Control Conference, 1988*. 1988.
12. Wu, Y., X. Yu, and Z. Man, *Terminal sliding mode control design for uncertain dynamic systems.* Systems & Control Letters, 1998. **34**(5): p. 281-287.
13. Maolin, J., et al., *Practical Nonsingular Terminal Sliding-Mode Control of Robot Manipulators for High-Accuracy Tracking Control.* Industrial Electronics, IEEE Transactions on, 2009. **56**(9): p. 3593-3601.
14. Tamaz, S., R. Gourdeau, and S. Martel. *Bidimensional MRI-based Navigation System Using a PID Controller*. in *Engineering in Medicine and Biology Society, 2006. EMBS '06. 28th Annual International Conference of the IEEE*. 2006.

15. Martel, S., et al., *Automatic navigation of an untethered device in the artery of a living animal using a conventional clinical magnetic resonance imaging system.* Applied Physics Letters, 2007. **90**(11): p. 114105-114105-3.
16. Tamaz, S., et al., *Real-time MRI-based control of a ferromagnetic core for endovascular navigation.* Ieee Transactions on Biomedical Engineering, 2008. **55**(7): p. 1854-1863.
17. Felfoul, O., et al., *<emphasis>In Vivo</emphasis> MR-Tracking Based on Magnetic Signature Selective Excitation.* Medical Imaging, IEEE Transactions on, 2008. **27**(1): p. 28-35.
18. Yong, F., Y. Xinghuo, and M. Zhihong. *Non-singular terminal sliding mode control and its application for robot manipulators*. in *Circuits and Systems, 2001. ISCAS 2001. The 2001 IEEE International Symposium on*. 2001.
19. Yu, S., et al., *Continuous finite-time control for robotic manipulators with terminal sliding mode.* Automatica, 2005. **41**(11): p. 1957-1964.
20. Jin, M., et al., *High-Accuracy Tracking Control of Robot Manipulators Using Time Delay Estimation and Terminal Sliding Mode.* International Journal of Advanced Robotic Systems, 2011. **8**(4): p. 65-78.
21. Chang, P.H. and S.H. Park, *On improving time-delay control under certain hard nonlinearities.* Mechatronics, 2003. **13**(4): p. 393-412.
22. Bohn, C. and D.P. Atherton, *An analysis package comparing PID anti-windup strategies.* Control Systems, IEEE, 1995. **15**(2): p. 34-40.
23. Chang, P.H. and J.W. Lee. *An Observer Design for Time-Delay Control and its Application to DC Servo Motor*. in *American Control Conference, 1993*. 1993.
24. Chang, P.H. and J.W. Lee. *Time delay observer: a robust observer for nonlinear plants using time-delayed signals*. in *American Control Conference, Proceedings of the 1995*. 1995.
25. Lee, J.W. and P.H. Chang. *Input/output linearization using time delay control and time delay observer*. in *American Control Conference, 1998. Proceedings of the 1998*. 1998.
26. Maolin, J., K. Sang Hoon, and C. Pyung-Hun, *Robust Compliant Motion Control of Robot With Nonlinear Friction Using Time-Delay Estimation.* Industrial Electronics, IEEE Transactions on, 2008. **55**(1): p. 258-269.
27. Arcese, L., M. Fruchard, and A. Ferreira. *Nonlinear modeling and robust controller-observer for a magnetic microrobot in a fluidic environment using MRI gradients*. in *Intelligent Robots and Systems, 2009. IROS 2009. IEEE/RSJ International Conference on*. 2009.
28. NHS Purchasing and Supply Agency. Report 06006 3T MRI Systems. Issue 4. May 2007

요 약 문

이 논문은 경로 추적을 위한 컨트롤 법을 설계한 것이다. 목표는 혈관 내에서 정확하게 마이크로 로봇의 움직이는 것이다. 마이크로 로봇은 강자성체 물질로 만들어져 있고 자기장에 의해서 추진 된다.

컨트롤러는 시간지연제어기법(time delay control)과 terminal sliding 컨트롤을 함께 사용하였다. TDC 는 플랜트에 대한 선행 지식 없이 적용할 수 있다. 시스템이 불확실함과 예상치 못한 외란을 포함하고 있는 비선형 일 때 TDC 는 모델 기반의 컨트롤러에 비해 적은 노력이 드는 장정이 있다. 한편, TSM 은 정확도를 더하여 TDC 의 주정에러를 보상하고 또한 매개변수의 변화와 외란에 반한 견고함을 더한다. 게다가 안티 와인드 업은 TDC 와 TSM 의 적분 때문에 축적되는 에러를 제거하는 역할을 한다. 제안한 컨트롤러는 와인드업 현상에 의한 작동기의 포화현상을 피할 수 있다.

시뮬레이션은 실제 현상을 따라 시행되었다. 정확도와 견고함 평가는 전체적인 컨트롤러가 어떻게 수행하는가를 보는 것과 각각 컨트롤 방법이 주는 개선점을 보는 단계로 실시하였다.

키워드: 마이크로 로봇, 궤적 추적, time delay control, terminal sliding mode